LAPPEENRANTA UNIVERSITY OF TECHNOLOGY
Faculty of Technology
Master's Degree Program in Mechanical Engineering

Mohammad Gerami Tehrani

ENERGY EFFICIENCY CONSIDERATION IN ELECTRIC VEHICLE TRANSMISSIONS

Examiners: Prof. Aki Mikkola
D.Sc. (Tech.) Kimmo Kerkkänen

ABSTRACT

Lappeenranta University of Technology
Faculty of Technology
Master's Degree Program in Mechanical Engineering

Mohammad Gerami Tehrani

Energy Efficiency Consideration in Electric Vehicle Transmissions

Master's Thesis
2013

95 pages, 36 figures, 5 tables and 7 appendixes

Examiners: Professor Aki Mikkola
D.Sc. (Tech) Kimmo Kerkkänen

Keywords: Efficiency Analysis, Electric Vehicle, Transmission Power Loss

This study is a survey of benefits and drawbacks of embedding a variable gearbox instead of a single reduction gear in electric vehicle powertrain from efficiency point of view. Losses due to a pair of spur gears meshing with involute teeth are modeled on the base of Coulomb's law and fluid mechanics. The model for a variable gearbox is fulfilled and further employed in a complete vehicle simulation. Simulation model run for a single reduction gear then the results are taken as benchmark for other types of commonly used transmissions. Comparing power consumption, which is obtained from simulation model, shows that the extra load imposed by variable transmission components will shade the benefits of efficient operation of electric motor. The other accomplishment of this study is a combination of modified formulas that led to a new methodology for power loss prediction in gear meshing which is compatible with modern design and manufacturing technology.

ACKNOWLEDGEMENTS

This thesis has been conducted in product development department of Valmet Automotive. The propose of this thesis was to investigate the efficiency of electric vehicle powertrain integrated with different type of transmissions. M.Sc. Juuso Kelkka from Valmet Automotive has been the instructor for this work. The examiners for this thesis were professors Aki Mikkola and Kimmo Kerkänen.

I want to thank M.Sc. Juuso Kelkka for providing this valuable opportunity and his specialist advice and guidance and his patience with my questions. I would also like to thank D.Sc. Markus Hirvonen, the project manager of product development at Valmet Automotive, for his wise leadership. In addition, I owe my experience and new understanding of electric vehicle to all of corporative and kind staff there.

Many thanks are due towards D.Sc. (Tech) Kimmo Kerkänen at Lappeenranta University of Technology for his responsive and compassionate supervision during my work. I should appreciate Professor Aki Mikkola for moral inspiration that I received.

Finally, I am very indebted to my mother who has been consistently giving me all the trust, support, and encouragement until now. My special thanks go to my beloved Masoumeh for her patience and backing.

Uusikaupunki, 16.11.2012

Mohammad Gerami Tehrani

TABLE OF CONTENTS

LIST OF TABLES

LIST OF FIGURES

NOMENCLATURE

Abbreviations

ABEC	Annular Bearing Engineers' Committee
ABMA	American Bearing Manufacturers Association
AC	Alternating Current
CVT	Continuously Variable Transmission
DC	Direct Current
EV	Electric Vehicle
EHL	Elasto-Hydrodynamic Lubrication
FTP	Federal Test Procedure
HEV	Hybrid Electric Vehicle
IM	Induction Motor
IVD	Infinitely Variable Transmission
Li-ion	Lithium ion
NEDC	New European Driving Cycle
PMSM	Permanent Magnet Synchronous Motor
SRM	Switched Reluctance Motor
SAP	Start of Active Profile

Symbols

A	Area
B	Face width of tooth (m)
D	Pitch Diameter
d	Diameter
d_b	Mean diameter of bearing, 0.5 (bore + outer diameter)
E	Modulus of Elasticity (GPa)
$\boldsymbol{f_0}$	Bearing lubrication factor
h_r	Thermally corrected film thickness (m)
h_m	Minimum film thickness (m)
I	Current (A)
i	0, 1, …, k
K_f	Thermal conductivity (W/mK)
$\mathrm{m_g}$	Gear Ratio
N	Number of teeth
n	Rotational Speed (rpm)
n	Vector normal to the surface
P_e	Electric Power (watt)
P_m	Mechanical Power (watt)
P	Pressure

$\mathcal{P}$	Pitch (m)
p	Diametral Pitch
R	Equivalent radius of curvature (mm)
Re	Reynolds number
r	Pitch Radius (mm)
r_s	SAP radius
$\boldsymbol{U}$	Voltage (V)
U	Velocity (m/s)
u	Surface velocity (m/s)
X_0	Bearing radial factor
Y_0	Bearing thrust factor
Z	Number of drawn teeth in oil bath
z	Viscosity–pressure index
α_n	Pressure angle
α	Pressure-viscosity coefficient
β	Helical angle, arbitrary angle
δ	Temperature-viscosity coefficient (1/K)
η_T	Total Efficiency
η_e	Electric Efficiency
η_m	Mechanical Efficiency ($N.s/mm^2$)

η_M	Dynamic Viscosity ($10^{-3} N.s/m^2$) (cP)
η_G	Gearbox Efficiency
θ	Temperature (K)
μ	Coefficient of friction
μ_X	Friction Coefficient
ν	Poisson's ratio
ν_0	Kinematic viscosity ($10^{-2} cm^2/s$) (cSt)
ρ	Radii of the curvature (mm)
ρ	Density (kg/m^3)
σ	Contact Ratio
ς	Relative Maximum Hertzian Pressure (GPa)
τ	Torque (N.m)
υ	Relative speed (m/s)
ω	Angular Speed (rad/s)

Subscripts

A	axial, addendum
a	tooth tip (addendum)
b	bearing, backlash
c	cavity
d	drag

e	entering components,end
eq	equivalent value
f	facial
g	gear
i	gear index
j	index of control volume
n	normal
o	base
0	ambient condition
p	periphery
p	pinion, pocketing
R	radial
r	rolling components, ratio
S	static
s	sliding components

Superscripts

-	Mean Value
´	Effective value
L	Laminar
T	Turbulent

1 INTRODUCTION

The utilization of electric propulsion in transportation has increased radically during last decade. This has increased the performance requirements of the power transmission in electric vehicles. The resurgence of current interest in the early part of the 21st century has been driven by both political and technological developments, namely a requirement to control global emissions and the emergence of new battery designs with improved specific energy, energy density and rechargability properties. [1]

Whilst the batteries should be carried onboard in the vehicle and there is limited space for them, the amount of energy is constrained in EVs. In order to exploit every single electron and minimize losses, optimization in mechanical parts as well as electronics is needed. Efficient operation of electric motor has more advantages beside the less energy consumption. Less heat generation and speed variation will increase the duty life of stationary and rotary components of the electric motor like winding, sealing, bearing etc. Transmission as one of the most effective component in powertrain is the category, which is investigated in this work.

Unlike internal combustion engines, electric motors can provide maximum torque at the very first moment of starting, and after passing transient speed with constant torque rapidly will state in a wide constant power zone. This characteristic of electric drives leaves no reason for adding any extra component to the drive train while the efficiency of electric motor is not one of the concerns of electric vehicle design. According to the electric motor efficiency map, constant power curves pass through different efficiency contours. That means although the power is constant during acceleration the efficiency varies at different applied torque and corresponding angular speed.

The purpose of providing these kinds of maps is to manage the torque and speed so that its corresponding power point on the map stays in most efficient contour. There are two general ways to reach this aim; one is designing an electric motor with the vast high efficient contours to cover the variation of load request, or keeping the electric motor in its most efficient point and adopting the applied load by an interface that can be a gearbox.

Since the efficiency map is almost symmetric in motor and generator mode, keeping electric drive in sweet spot not only reduces the losses but also will increase the regeneration efficiency.

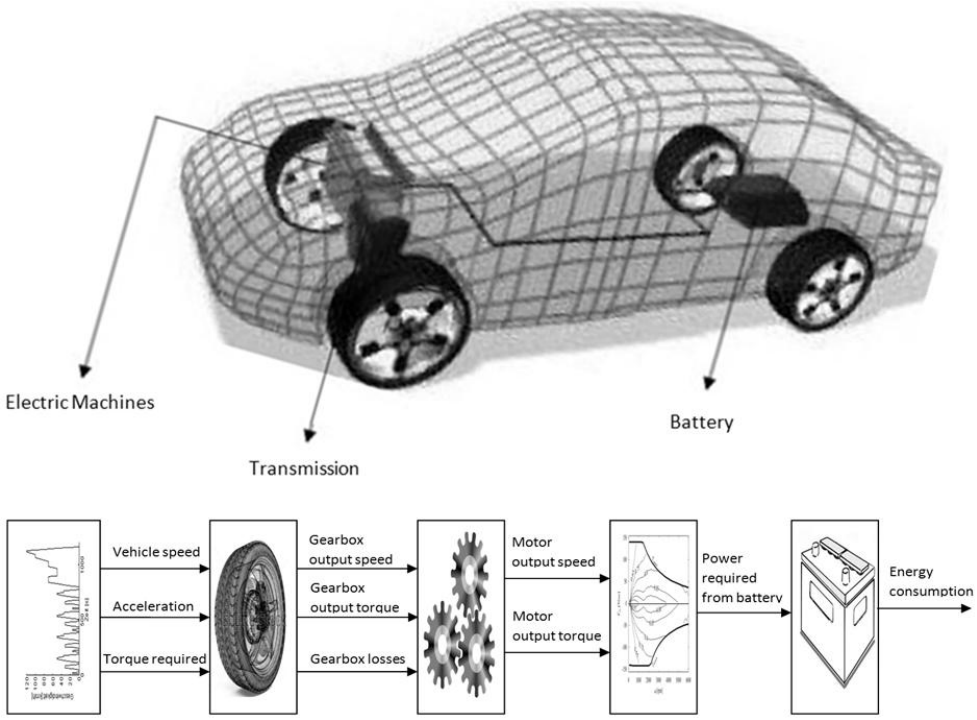

Figure 1.1. Electric Vehicle power sequence

There are different driving cycles what are gained through different traffic modes and various urban architectures. The main driving cycle patterns, which are currently used for designing cars, are New European Driving Cycle (NEDC), USA Federal Test Procedure (FTP) and Japan 10-15 mode. These driving cycles are the input for emission test or performance simulation.

The power consumption trajectory in electric vehicles starts from batteries and ends up with wheels (Figure 1.1). According to the applied driving cycle, demanded power is taken from the batteries in electric mode:

$$P_e = IU \tag{1.1}$$

Where P_e is electric power, I is current and U is voltage and due to electric machines converted to mechanical mode:

$$P_m = \tau\omega \tag{1.2}$$

Where P_m is mechanical power, τ torque and ω angular speed. Passing through gear(s), wheels are pivoted and run the car. In each stage, a percentage of power is lost related to that section efficiency. Total efficiency in electric vehicles is defined:

$$\eta_T = \eta_e\eta_m = {}^{P_m}/_{P_e} \times 100 \tag{1.3}$$

In order to increase the total efficiency of electric vehicle, increasing the efficiency of both electrical and mechanical components should be done in a way that encloses the mechanical power of wheels to the electrical power that is taken from batteries. There is a critical fact in discretized efficiency chain that modifying one stage efficiency should not compromise the total efficiency, because losses are not fixed all the time and relatively are varied by physical characteristics (speed, heat, friction etc.) of whole system.

Although there are some other electronic reasons which make it feasible not to exceed the nominal operating point in electric motors, this work is only focused on mechanical point of view. Furthermore electric drive type, size, cost, capability, etc. are other factors which give the transmission an essential role in an efficient design manipulation. Bringing forth a compatible coupling both electric motor and transmission specifications should be investigated before any draft.

In order to predict the mechanical power losses, power dissipation due to transmission and its component needs to be investigated precisely. The main objective of this study is to analyze verity of power loss in different shapes that happens in vehicle gearbox and

specifically in mechanical mode. A mathematical model is offered for power losses due to direct interaction between the gear and the pinion and its auxiliary effects on supporting bearings. Other losses such as mechanical vibration that leads to noise and heat and sealing friction etc. are neglected because their minor effect comparing to other issues.

However many improvements have done in chemical ingredients of batteries and variety of battery type has been developed to achieve longer range in EVs and HEVs, applying an electric motor in an efficient way by the means of an efficient transmission still increasing the vehicle trip range. The transmission ratio amplifies the output torque of the transmission, yet the transmission efficiency (η_G) reduces the net output torque. Thus, according to this term, application of the electric vehicle must be taken into account during designing the powertrain.[2]

Electric machine is one of critical components in a Hybrid Electric Vehicle (HEV). The aim of designing for such applications is to maximize efficiency over wide torque/speed range, which achieves adequate inertia of rotating parts to avoid compromising drivability of the vehicle and come up with compact package. According to electric machine principles, having bigger torque at low speed demands an electric motor what is heavy, large sized, expensive, etc. For avoiding these drawbacks and less earth sourced material usage, applying a high speed -low torque electric motor is reasonable while the power is still the same.

Different types of transmissions are already used in EVs and HEVs which have their own benefits and disadvantages. Basically, the transmission design refers to the type of vehicle which can be sedan, SUV, truck, etc. and their motion parameters like torque, power, maximum speed and acceleration.

In order to manage all electrical and mechanical factors to provide a general manner for transmission design in EVs and HEVs it is needed to provide information about different gearbox structures which are used so far and evaluate their benefits and drawbacks. Creating a simulation model respecting to the gearbox fundamentals and verify it by evaluating the real life measurement values is the one of the goals. Comparing the actual values with the virtual outputs from the simulation model will help to revise the simulation

theory and defining coefficients to get it as precise as possible. Then by the mean of a reliable simulation, various engagements of different electric motors and different gearboxes can be assessed in order to find the most efficient combination for demanded applications.

In electric motors designing, there are three major factors which take into account: Maximum torque, maximum speed and base speed. Since each of these factors affect the motor characteristics such as dimension, geometry, weight etc. in order to satisfy the operator demands, these factors should be manipulated to make the electric motor suitable from both electrical and mechanical aspects.

In order to utilize a simple electric drive with a narrow rotational speed variation range, a gear set is needed to cover vehicle low speed and high speed loads. Though electric motors seem to operate in a constant power in the majority of time, applying a gear set also makes it possible to keep the electric motor working point in the sweet spot where the efficiency is higher according to the corresponding torque and speed.

Finding a solution how to apply an electric motor integrated with a variable gearbox rather than a sole electric motor to increase the battery to wheel efficiency without compromising the electric vehicle performance and efficiency for different vehicle category is the objective of this thesis work. In this thesis, unlike similar studies, power losses due to the geartrain is also have taken into account during the total efficiency calculation.

This report is fulfilled according to the Valmet Automotive® plan for expanding the performance and efficiency of pure electric vehicles by the means of company properties and benchmarks. The details in the tests are limited due to corporate secrecy. Some describing pictures, details and full chapters have been removed due to corporate secrecy.

2 THEORY

2.1 Background

Since using the electric vehicle as an ordinary transportation mean is almost a new phenomenon now days, there are many different ideas about it because an EV is a combination of electrical and mechanical science. Many changes have happened since the mid-19th century when the first electric car made. As the electricity can be kept in battery cells, only DC power is available in EVs and because the high performance and long duty life are demanded in cars, DC motors couldn't survive any longer and DC~AC inverters applied to adopt the power supply to AC motors which are cheaper, more reliable, more powerful and maintenance free.

Electricity must be stored in EVs in a way that makes it possible to run it in long distances; consequently, a new system of batteries is needed. Lithium-ion (Li-ion) batteries, which are commonly used in many applications, are suitable for electric vehicle (EV) applications because of their relatively high energy densities per mass, volume, and cost unit. The lithium-based chemistries have three times the energy density of other kind of batteries. An innovation in recent HEVs so-called "Range Extender" is a combination of a small engine integrated with a generator charging the batteries when they get depleted and makes them capable of running more than what is defined by the capacity of batteries.

Beside of improvement in battery, converter, electric motor, etc. almost none of pure electric vehicles are applying variable transmission. Although there are some studies about integrating different kind of ideal gearboxes with powertrain and its positive effect has been proved, according to this believe that electric losses are less than mechanical ones, carmaker companies prefer to design the power train for specific application with no need of gear shifting.

This way of mentation caused a conservative strategy in car factories those invested in EVs, and it is wise not to take more risk while the market is not sure and making such a car in small number is expensive.

2.2 Electric Drives

The most common electric motor type that uses in EVs in mass production is PMSM (Permanent Magnet Synchronous Motor) though varieties of other electric motors are applied in EVs. Induction motors and reluctance motors are the other kinds of electric motor what are utilized in EVs, but they are restricted in concept cars and low volume production.

The induction motors are characterized by simple construction, reliability and low maintenance costs and they are able to operate in hostile environments. Nonetheless, they are characterized by a lower efficiency when compared to the permanent magnet motors, due to their rotor losses.

Switched reluctance motors have been gaining much interest as a candidate for applications in electric vehicles, because of its simple and rugged construction, simple control and ability of extremely high-speed operation. However, these motors also show several disadvantages: they have noise problems; and they are characterized by a lower efficiency when compared with permanent magnet motors. [3]

A small electric motor with high nominal speed is not capable of responding to a wide range of torque variation only with a single reduction gear. If the electric motor exceeds its nominal rotational speed, it will not function as its defined operating characteristics any more. “Field weakening” in PMSM, “slip” in induction motors and “torque ripple” in reluctance motors are the phenomena that cause failure due to over speeding the electric drives. In order to match the vehicle performance with moderate size electric drive and eliminating the torque change restrictions, vast variety of reduction gears are used. [4]

Except of hub electric motors that are mounted on vehicle drive shaft, other kind of EVs are using an interface between propulsion source and wheels. The interface can contain a reduction gear also. In EVs, which are applying only one electric motor for running wheels, differential usually plays the reduction gear rule as well.

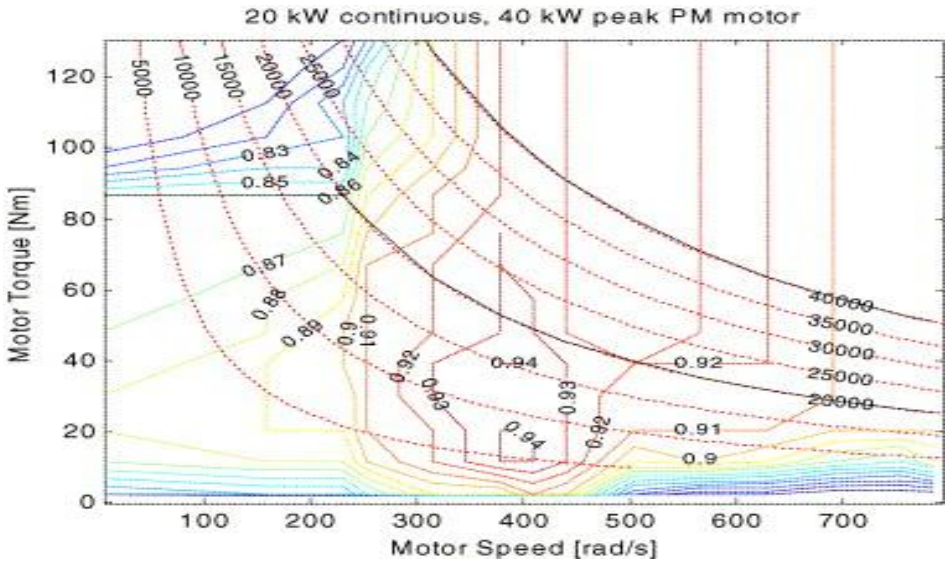

Figure 2.1. Typical electric motor efficiency map [1]

In the common believe about electric motors characteristics, which they can provide constant power in a wide variety of rotational speed, the heat, friction and copper losses are showing up due to increasing the speed, so the constant power curve does not exist in reality. Another fact about electric motors is the efficiency that is the most concerning point in EVs. According to actual experiments, electric drives have different efficiencies at different working points (*Figure 2.1*).

2.3 Geartrain

Two common gearhead or reducer designs are spur and planetary. In general, spur gearheads are simpler and less expensive than planetary units and work best for low-torque applications. Torque capacity of spur types is limited because each gear in the train bears the entire torsional load. Planetary gearheads, in contrast, share the load over multiple planet gears. While the input and output torque can be carried out through any planetary gear set, for reduction purposes, the input shaft drives a central sun gear that, in turn, drives the planet gears. Each of the planet gears simultaneously deliver torque to a rotating carrier plate coupled to a geared output shaft.

Furthermore, adequate lubrication is important, especially at high speeds and loads. Here, planetary gearheads have the advantage because oil flying outward from the sun gear have been captured by the planet gears and carrier plate. Spur types, on the other hand, tend to fling lubricant off and away from the gears. This is one reason planetary gear-heads have higher speed ratings.

Next, consider backlash and reduction ratio. Backlash is a measure of positional accuracy usually specified in arc-minutes. For example, a typical spur gearhead has about 10 arc-min of backlash, whereas its planetary counterpart may have about half of that. Reduction ratios for both spur and planetary gearheads range from near unity up to several hundred to one. Spur gearheads, with a single geared input shaft coupled to a geared output shaft (single stage), provide about 6:1 reduction. Planetary units, for comparison, can reach roughly 10:1 in a single stage. For higher ratios and proportionally greater output torque, multiple stages or gear sets are stacked together axially. Increasing the number of stages boosts the reduction ratio and output torque but increases overall length and lowers mechanical efficiency.

Whilst in spur gear meshing, output driveshaft has to split parallel and eccentric from the input, in planetary geartrains the output and input shafts are concentric and it makes it more symmetric which brings more facilities in powertrain design.

Planetary gear trains are complex critical components of several electromechanical systems such as wind turbine, aircrafts, automotive, gas turbines and numerous more heavy-duty industrial applications. As mentioned above, planetary gearboxes have several advantages compared to simple parallel gears, including their higher power density, lower gear noise, multiple speed ratios and compact size. Accordingly, in order to increase efficiency and to decrease size and cost, planetary gearboxes are becoming more and more popular. [6]

Geartrain should be designed so that keeps the electric motor operation in the “sweet spot”. The term “sweet spot” refers to the contours in the electric motor efficiency map that have

closest value to 100 % (Figure 2.1). According to above mentioned, planetary gear sets are the most proper option for designing a transmission for electric vehicles.

In gear meshing with involute teeth type there are three sequences in each engagement, which are before, after and at the centerline (Figure 2.2). Applied pressure is increasing from the first moment that driver and driven gear tooth meet each other and the maximum pressure happens in centerline which is called operating point. Amount of force in between will decrease while teeth are departing.

As shown in (Figure 2.2), if touching points are connected to each other they will build a straight line that is the tangential line on gears base circle and called line of action and its horizontal angle with is pressure angle (α_n). In addition, operating pitch circle is the trajectory of operating point in gear revolution.

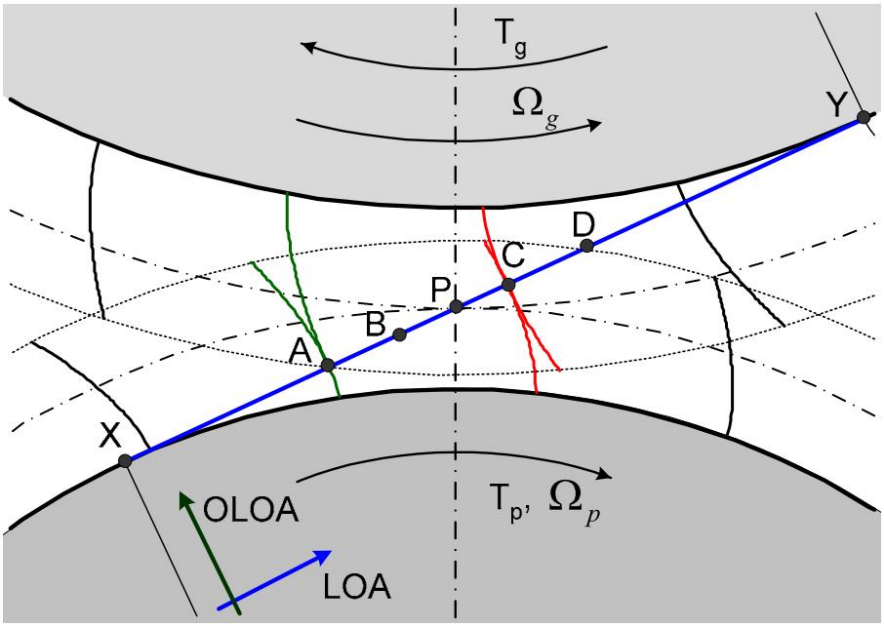

Figure 2.2. Involute toothed gear-meshing sequences [9]

According to the introduction, the proper choice for an EV transmission is the epicyclic gear set. Epicyclic or commonly known, planetary gear is a form of gear setup which is usually applied in high torque conveys demands in a compact package. There are several different kinds of epicyclical gears available, depends on how much torque is needed to

deliver at which speed. The number of planets is defined by demanded power, more planets increases the capability and robustness of gearbox.

The number of planets should not be lower than three because of stability although is possible to build it by only one planet. The most common setup is the three and four planet gear types. The gearbox that considered as sample in this thesis is simple spure gears which can be developed later in each part of an epicyclic gearset. A single stage can achieve a ratio of approximately ten, although sometimes an even higher ratio is required. In order to achieve this higher ratio two or more stages can be mated in an enclosure creating a gearbox with variable gear ratio and axis rotational direction. The planetary gear stage generally consists of four different parts (Figure 2.3).

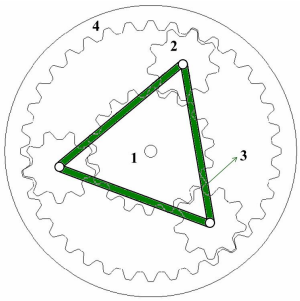

Figure 2.3. Typical 3 wheel planetary gear set

1. Sun gear (center) S

2. Planet gears (three gears rotating around the Sun gear) P

3. Planet carrier (holds the planetary gears in place so the gear does not jam) C

4. Annulus (inner toothed ring gear) R

There are four main combinations and output ratios in a planetary gearset depending on which part is pivoting or kept stationary. By adding more (n) stages more combination and ratios (4^n) are available. Since in epicyclic gearset, which are integrated with electric motors, reduction, ratio is desired. Generally, the ring gear is fixed to the housing, sun is

gear, planet is pinion and output shaft is connected to planet carrier. Different combinations of a single stage of planetary gearbox are described in the table blow: [7]

***Table* 2-1** Possible combination in planetary gearset

	Input	**Stationary**	**Output**	**Ratio**
i	Sun	Ring	Planet carrier	$1 + (\frac{R_R}{R_S})$
ii	Planet carrier	Sun	Ring	$\frac{1}{(1 + (\frac{R_S}{R_R}))}$
iii	Sun	Planet carrier	Ring	$-\frac{R_S}{R_R}$
iv	All	Planet	All	1

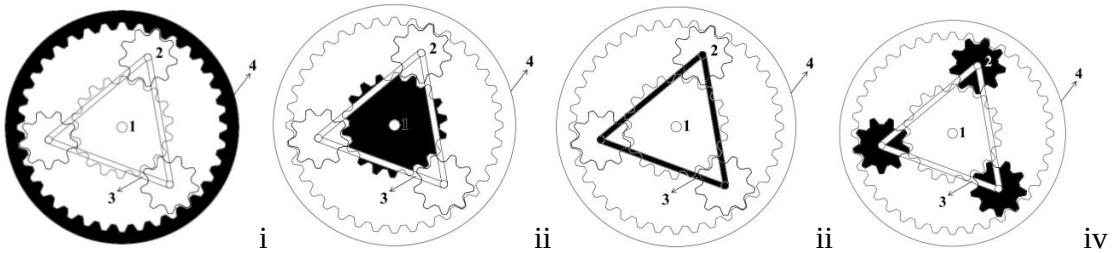

i ii ii iv

Analyzing gear meshing equations in an epicyclic setup can be done by separating components and modifying spur gear equations for each engagement. Then by superposing the effects in all segments, a general solution will achieve. Since transmissions power losses calculation is one of the objectives of this work the final general relation should be a function of power that means force (torque) and speed (frequency). [16]

Considering two meshing gears below is provided as an example of a typical component in an epicyclic gear. The two gears and the arms are rotating as shown Table 2-1.

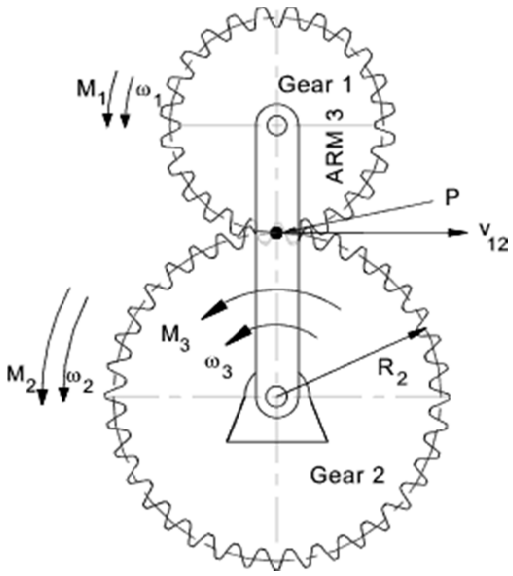

Figure 2.4. Schematic epicyclic gear [8]

Now it the arm was stationary the contact point P would have an instantaneous velocity = -$\omega_2 R_2$. (Velocities to the right are positive). Now if the whole system was rotating as a rigid assembly with the velocity of the arm the instantaneous velocity -$\omega_3 R_2$. Combining these two motions together, the linear velocity of the tooth engagement ($Gear_2 > Gear_1$) is therefore:

$$V_{12} = (\omega_2 R_2 - \omega_3 R_2) = -(\omega_2 - \omega_3) R_2 \tag{2.1}$$

Now the magnitude of the transmitted tangential force (F_{12}) multiplied by the tooth engagement velocity (V_{12}) is equal to the potential power and the power loss due to tooth friction is proportional to this power. Generally, for spur gears (and helical gears) it is sufficient to estimate the power loss as 1% of the potential power. For more accurate estimations the equations below can be used: [8]

$$P = 0.01\, F_{12} V_{12} \tag{2.2}$$

The potential power is not the actual power but is the power transmitted by the same gears operating on fixed centers at angular velocities of (ω_2 - ω_3) for gear 2 and (ω_1 - ω_3)for gear 2.

The actual pitch line velocity of the gear mesh is - (ω_2) and therefore, the ration of the potential power to the actual power is:

$$\frac{Potential\ Power}{Actual\ Power} = \frac{F_{12}R_2(\omega_2 - \omega_3)}{F_{12}R_2(\omega_2)} = 1 - \frac{\omega_3}{\omega_2} \qquad (2.3)$$

2.4 Mechanical Power losses

Defining losses in EVs transmission as a function of torque and velocity makes it possible to determine losses through electric motor efficiency map with corresponding points and finally the comparison between geared and gearless EV in total efficiency. The mechanical losses of the gearbox generally can be divided into 3 different sub losses. Losses are: [5]

- meshing losses
- support bearing losses
- windage losses

According to “Comparison of spur gear efficiency prediction methods” (Anderson & Loewenthal, 1981) which compared five different methods for power loss prediction in spur gear meshing (methods of Anderson and Loewenthal, Buckingham, Chiu, Merritt, and Shipley) and evaluating the reliability of them in different working points and boundary conditions, Anderson & Loewenthal method is chosen as base of calculations. Even though the report is done in 1981 and new methods provide higher efficiency and power losses, the method and coefficient definitions are still reliable for modeling different gearboxes.[11]

Since the aim of this thesis is investigating the gearbox losses effect on whole powertrain system, not gear designing, so only the result of Anderson & Loewenthal report is taken for modeling the system.

In this report, the system is lubricated by oil jet and assumed that gears are not drawn in an oil pool. Furthermore, oil splashing which causes momentum losses due to oil drop departure and vibration losses which are making noise have not taken into consideration. The windage and bearing losses can be calculated in a straightforward manner with approximate expressions. The mesh losses are more complex and are analyzed in detail. Whilst the preconditions of Anderson & Loewenthal report are applicable in an EV gearbox for initial designing, in some parts rough estimations are done for this work accordingly.

2.5 Load Dependent Losses

As mentioned above, power losses in gear meshing are mainly divided into sliding component in frictional form (P_S) and rolling component in hydrodynamic form (P_R). Sliding losses are based on friction between tooth surfaces where the friction coefficient (μ_s) is the main factor. The hydrodynamic rolling (or pumping) loss is the power required to draw and compress the lubricant to form a pressurized oil film which separates the gear teeth in order to make the contact surface smoother and more slippery. According to following calculations it can be seen that at light loads the rolling traction loss is a major portion of the system loss.

In gear type power transmission, input load is conveyed while gear teeth are pulling each other. Although tooth surfaces are looking plain and fully burnished in macro view, they are ragged surfaces and asperities are resisting against each other to slide and a portion of power will lose in heat, wear and noise form. In order to minimize this loss a lubricant is applied in between. The lubricant film thickness varies according to amount of pressure applied on it that may even be eliminated in extremely high pressures. So there are three types of lubricant film which are dry sliding, fully lubricated sliding and semi lubricated sliding. The mean pressure level determines lubricant type and viscosity. It must be seen

that although using lubricant fluid with high viscosity results in thicker films and decreases the friction coefficient it will increase the rolling (pumping) resistance.

In order to calculate the friction coefficient, variety of modeling like: Coulomb Model, Benedict and Kelley Model, Xu's full Model and Smoothened Coulomb Model, have done so far. Regarding to 'Comparison of Spur Gear Efficiency Prediction Methods', all methods except Merritt's predict the same sliding power loss when the same friction coefficient is used so friction coefficient is crucial in sliding power losses calculation. Thus, in this work the new formulation which is suggested by Xu is utilized for calculation of friction coefficient and friction type assumed fully lubricated all the times. [9, 12]

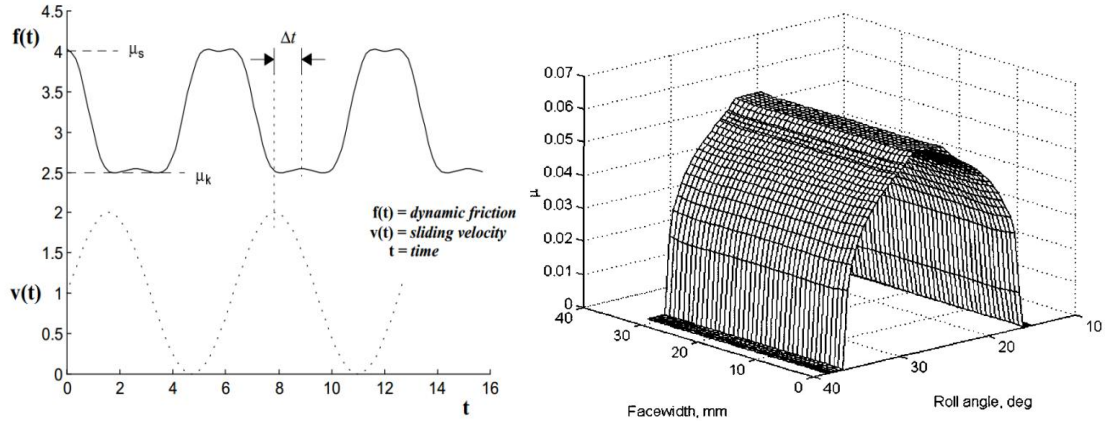

Figure 2.5. Typical variation in μ over the entire surface of spure gear tooth [13, 14]

If the friction coefficient is defined properly, all the different methods will bring almost similar results. Since applied load varies on each tooth during the meshing cycle, the friction coefficient has different instantaneous value versus time. Thus the friction coefficient would be a function of time (Figure **2**.5). The rule of friction coefficient is significantly affective while the losses are varying proportionally to the carried load. [10]

According to "Neil E.Anderson and Stuart H.Loewenthal" report, if we assume that during the mesh cycle, the load transmitted between the gears is normally carried by either one or two teeth at any time, term of "contact ratio" (σ), which is the average of engaged teeth, will be two, thus Meshing cycle is divided in to 4 phases (Figure 2.6):

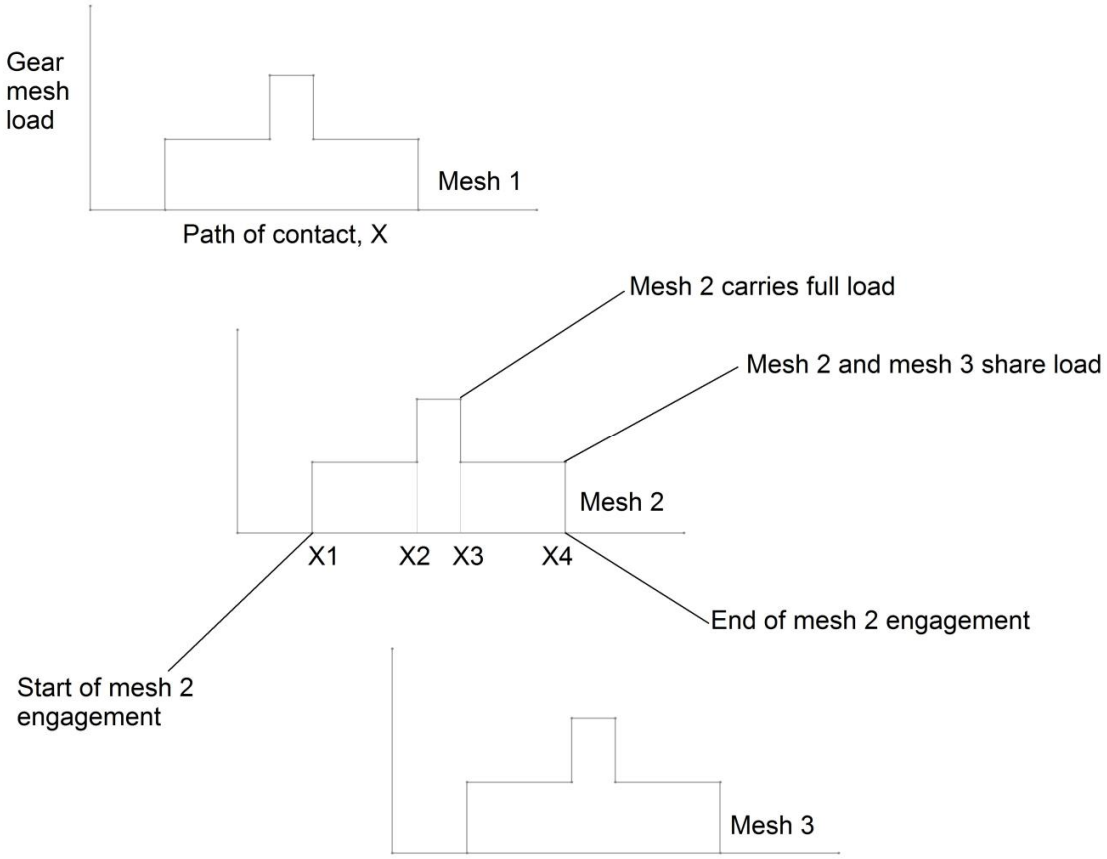

Figure 2.6. Sharing on teeth sequences [15]

X_1- Start of mesh cycle, two teeth share the load

X_2- start of single-tooth contact

X_3- End of single-tooth contact

X_4- End of mesh cycle

X_P- Pitch point

In order to have the average power losses during mesh cycle regarding to cycle division for both sliding and rolling losses, discretized integrating in each sequence is done and since

the duration of single-tooth engagement is about one fifth of whole mesh cycle, each integral is weighed by its portion:

$$\bar{P}_S + \bar{P}_R = \frac{1}{X_4 - X_1}\left\{2\int_{X_1}^{X_2}[P_S(X) + P_R(X)]dX + \int_{X_2}^{X_3}[P_S(X) + P_R(X)]\,dX + 2\int_{X_3}^{X_4}[P_S(X) + P_R(X)]\,dX\right\} \quad (2.4)$$

2.5.1 Sliding Losses

The basic Coulomb Law of friction can be used to define the resistive force between two involute spur gear teeth. Since the amount of carried load and portion of sliding and rolling in type of contact is not fixed and varies by time so equation terms should be a function of time.

$$F_X(t) = \mu_X(t)w_X(t) \quad (2.5)$$

Where F_X is frictional resistive force, μ_X is friction coefficient and w_X is normal load on sliding surfaces. Regarding to (Figure 2.6) and discretized gear mesh cycle into $X_1 \dots X_4$, Sliding power losses with thermal correction coefficient can be derived as blow:

$$P_s = C_3V_s(X)F_s(x) \quad (2.6)$$

Where P_s is sliding pressure, C_3 is constant from table **Table 6-1** and V_s is teeth surface sliding speed In order to calculate sliding power losses, sliding force and speed should be calculated concentrating on pure sliding force and relative sliding surfaces velocities. Expanding Coulomb's law terms, by a combination of Xu's suggested method for

coefficient of friction [19] and Anderson & Loewenthal's report that linearized mesh cycle, applied for this power loss compartment.

Applying vector algebra is easier to define geometrical values for calculating relative radius, speed and curvatures between two gear teeth. This also makes it possible to decrease the variables in equation and easier to understand derived relations.

Calculating the friction coefficient in this study is based on Xu's method but some minor changes have been done in variables and discretization is done according to Anderson & Loewenthal's method.

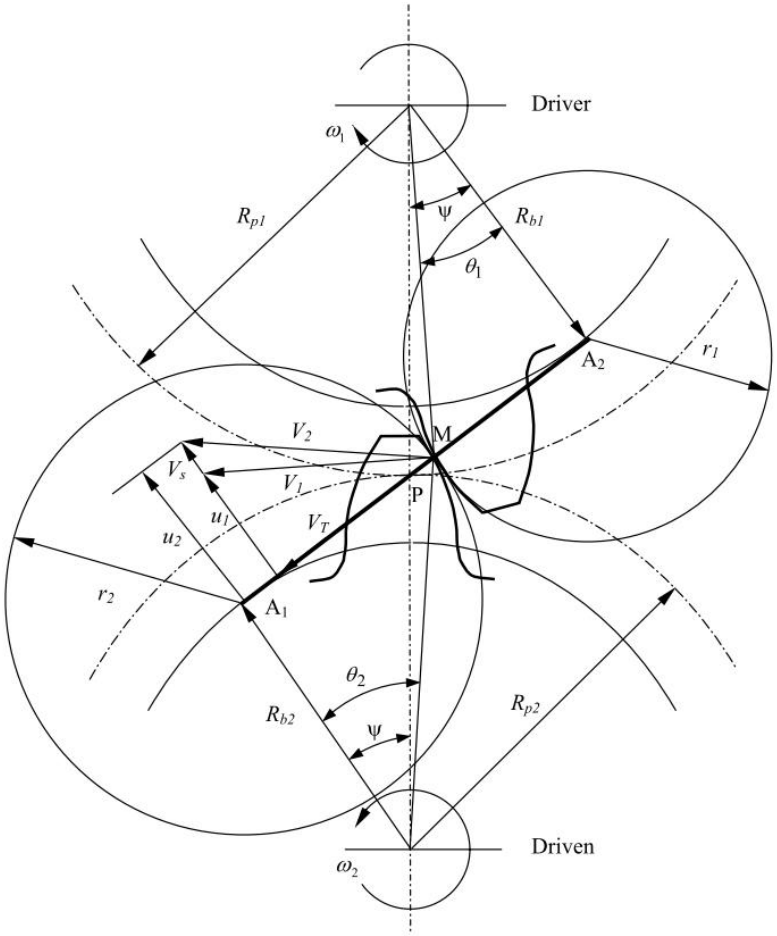

Figure 2.7. Spur gear geometry used for calculation of curvatures and surface velocities [20]

General Xu equation for μ is rectified by a sign function to neutralize the effect of friction direction fluctuating during mesh cycle, which is positive and negative before and after pitch point.

$$\mu_{Xi}(t) = e^{f^*} P_{hi}^{b_2} |SR_i(t)|^{b_3} V_{ei}^{b_6}(t) \eta_{oil}^{b_7} R_i^{b_8} . sgn\left[mod\left(\Omega_p r_{bp} t, \mathcal{P}_o\right) + (n-i)\mathcal{P}_o - L_{AP}\right] \quad (2.7)$$

$$f^* = f\left(SR_i(t), P_{hi}(t), \nu_o, S_{avg}\right) = b_1 + b_4 \varsigma + b_5 e^{-\varsigma} b_9 e^{S_{avg}} \quad (2.8)$$

Where ν_o, is kinematic viscosity of lubricant and S_{avg} is surface roughness average.

$$\left\{\begin{matrix} b_1 = -8.916465, b_2 = 1.03303, b_3 = 1.036077, b_4 = -0.354068, b_5 = 2.812084 \\ b_6 = -0.100601, b_7 = 0.752755, b_8 = -0.390958, b_9 = 0.620305 \end{matrix}\right\}$$

f^* is substituted for above equation to summarize main friction coefficient equation.

$$\varsigma = |SR_i(t)| P_{hi}(t) \log(\eta_M) \quad (2.9)$$

Where η_M is dynamic viscosity and for shortening the equation relative maximum hertzian pressure (P_{hi}) between teeth separated and it is easily understandable from (2.7), (2.8) that while the slide to roll ratio (SR) is decreasing, the effect of hertzian pressure and consequently friction coefficient will decay exponentially.

$$SR_i(t) = 2\frac{u_p(t) - u_g(t)}{u_p(t) + u_g(t)} = 2\frac{v_{si}(t)}{v_{ei}(t)} \quad (2.10)$$

Where u_p and u_g are absolute speed of pinion and gear tooth surface and v_s refers to relative sliding speed Slide to roll ratio is a determinant factor to diagnose whether teeth are sliding or rolling over each other.

$$v_{si}(t) = \frac{0.1047(1 + m_g)n_p(X - X_p)}{m_g} \tag{2.11}$$

Since Anderson & Loewenthal study is based on overall loss calculation, continuous-time is discretized into t_1 to t_4 and time is illustrated by X instead. That is why the right side of equation is time excluded.

$$v_{ei}(t) = 0.1047 n_p D_p \left[sin\, \alpha_n - \frac{|X - X_p| - (m_g - 1)}{D_g} \right] \tag{2.12}$$

Equation above refers to entraining component velocity and with a good approximation achieved by relative rolling speed.

Whilst spur gear teeth profile designed in a way to make the mesh type in rolling fashion all the times, normal imposed load in between can be regarded as two parallel rolling cylinders and the equation suggested by Heinrich Hertz applied:

$$\frac{1}{E'} = \frac{1 - \nu_p^2}{E_p} + \frac{1 - \nu_g^2}{E_g} \longrightarrow E' = \frac{2}{\left(\frac{1 - \nu_p^2}{E_p} + \frac{1 - \nu_g^2}{E_g}\right)} \tag{2.13}$$

Effective modulus of elasticity introduced by K. L. Johnson and K. Kendall and A. D. Roberts, (1971) [22] utilized in Hertz's equation which combination of modulus of elasticity of engaged gear teeth (E_p, E_g). In this case, because variable radius of curvature instead of diameter is used factor 2 is illustrated on numerator.

Respectively maximum hertzian pressure is a function of normal load, modulus of elasticity and radii of curvature of bodies in contact. In spur gear tooth profile, curvature radius is varying by time and it can be seen from equation (2.3) the sharper contact surface is the higher hertzian pressure.

$$P_{hi}(t) = \sqrt{\frac{w_n E'}{2000\pi R_{eqi}(t)}} \tag{2.14}$$

The gear tooth profile in addendum part has a significant effect on hertzian pressure and according to S. Baglioni, F. Cianetti, L. Landi [21] study; addendum modification can improve the efficiency up to 0.5%.

Defining radii of curvature in discretized mesh cycle for pinion and gear is defined as below:

$$\left.\begin{aligned} \rho_p &= r_p \sin\theta + |X - X_p| \\ \rho_g &= r_g \sin\theta - |X - X_p| \end{aligned}\right\} \tag{2.15}$$

Again, from K. L. Johnson and K. Kendall and A. D. Roberts, (1971) [22], equivalent radius (R_{eq}) is achieved as below:

$$\frac{1}{R} = \frac{1}{\rho_p} + \frac{1}{\rho_g} \longrightarrow R_{eq} = \frac{\rho_p \rho_g}{\rho_p + \rho_g} \tag{2.16}$$

Since during mesh cycle entraining (rolling) components are seen at same parallel speed in opposite direction, absolute velocity of entraining components is equal to half of relative velocity:

$$V_{ei}(t) = \frac{v_{ei}(t)}{2} \tag{2.17}$$

Main factor that not only affects the sliding and rolling friction losses but load independent losses, is teeth surface roughness that is very critical in calculating lambda (Λ). Mean value for surface roughness can be obtained by simple averaging formula and also root mean square method, whatever used, in order to calculate total average value [appendix C], initial way should be followed. In this study RMS value of surface roughness have taken into calculations[27]:

$$S_{ave} = \sqrt{S_{rms,p} + S_{rms,g}} \tag{2.18}$$

The averaged surface roughness unit used is in micrometer (μm) and represents the mean value of surface asperities. The other parameter in Elasto-Hydro dynamic Lubrication (EHL) is minimum lubricant film thickness:

$$h_m = 3.07 \frac{(\eta_M + V_{ei})^{0.71} \alpha^{0.57} R_{eq}^{0.4}}{E'^{0.03} \; w^{0.11}} \tag{2.19}$$

Where w is normal load applied on counteracting surfaces. According to ISO/TR 1281-2, 2008, pressure viscosity coefficient α can be calculated by the kinematic viscosity ν_0 in $cm^2/_S$ as:

$$\alpha = 0.1122 (\frac{\nu_0}{10^4})^{0.163} \tag{2.20}$$

According to manufacturing process table for surface roughness, involute teeth contact can be seen as “Roller Burnishing” but it must define precisely to have an accurate Λ.

$$\Lambda = \frac{h_m}{S_{avg}} \tag{2.21}$$

Comparing various models for prediction of μ resulted in selecting Xu's Method that is the most efficient way. Applying Xu's model is restricted to after processed tooth surfacing in order to keep Λ in the range between one and three ($1 < \Lambda \leq 3$). In the other cases conventional formulas for coefficient of friction can be used such as Smoothened Coulomb Model for and Benedict and Kelley Model. [24]

$$\left.\begin{aligned} w_t &= \frac{T_p}{r_p} \\ w_n &= \frac{w_T}{\cos\alpha_n \cos\beta} \end{aligned}\right\} \longrightarrow w_n = \frac{2T_p}{D_p \cos\theta \cos\beta} \tag{2.22}$$

Whilst contact ratio (σ) is assumed to be 1.5 thus between $X_1$and X_2 and between X_3 and X_4 the load is shared by two gears. Between points X_2 and X_3 along the path of contact, w_n is carried by one tooth. Thus:

$$w(X) = w_n \qquad X_2 \leq X \leq X_3 \tag{2.23}$$

Normal force on sliding faces when one tooth is carrying the entire load is equal to conveying torque due to pinion. For the rest of mesh cycle it assumed that load is equally distributed on tow teeth so half of whole torque affects the friction resistance.

$$w(X) = \frac{w_n}{2} \qquad \begin{cases} X_1 < X < X_2 \\ X_3 < X < X_4 \end{cases} \tag{2.24}$$

For the rest of mesh cycle it is assumed that load is equally distributed on two teeth so half of whole torque affects the friction resistance. Base pitch term is defined as:

$$\mathcal{P}_o = \frac{\pi D_o}{N} \tag{2.25}$$

Where D_o is pitch base diameter and N is number of teeth. According to (Figure 2.2) it is geometric length between point A and point P (L_{AP}) and it is equal to half of total mesh cycle (ℓ_6 appendix B). So according to Anderson & Loewenthal:

$$L_{AP} = {}^{\ell_6}/_{2} \tag{2.26}$$

Instantaneous tangential sliding velocity basically is a function of pinion rotational speed and equivalent radii of curvature to its corresponding mesh cycle sequence:

$$V_S = 0.10472\, n_p \left(1 + \frac{1}{m_g}\right)(X - X_P) \tag{2.27}$$

Now, sliding power losses can be calculated by equation (2.6) which is independent of time.

2.5.2 Rolling Losses

Simultaneous rolling and sliding takes place between the tooth flanks of two mating gears, except at the pitch point, where pure rolling takes place. As explained by Xu [19], three different regions could be roughly defined on a μ versus SR curve. When the sliding velocity is zero, there is no sliding friction, and only rolling friction (though very small) exists. Thus, the μ value should be almost zero at the pitch point. When the SR is increased from zero, μ first increases linearly with small values of SR. This region is defined as the linear or isothermal region. When the SR is increased slightly further, m reaches a

maximum value and then decreases as the SR value is increased beyond that point. This region is referred to as nonlinear or non-Newtonian region. As the SR is increased further, the friction decreases in an almost linear fashion; this is called the thermal region. [18]

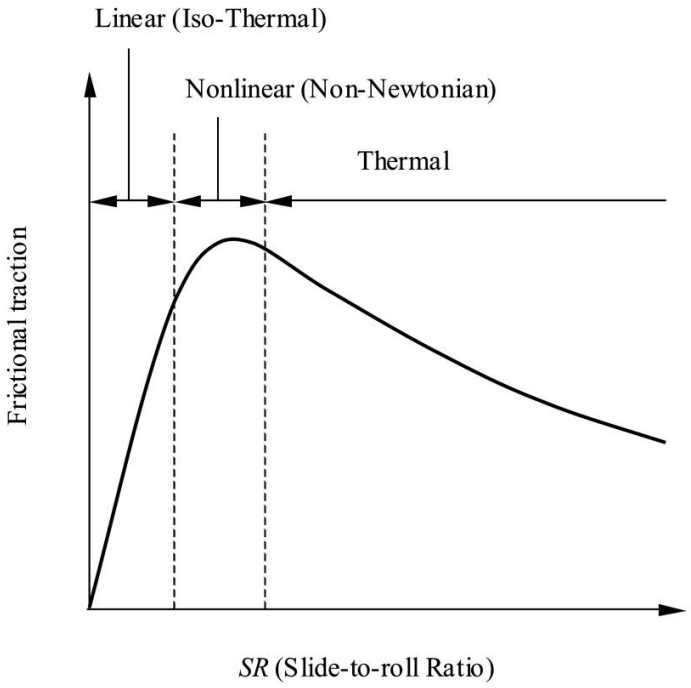

Figure 2.8. A typical μ versus SR curve [20]

The compression due to teeth pressure on each other tries to eliminate the oil film in between but while lubricant film stretches, because of molecular cohesion, which is called viscosity, it resists against and behaves like a spring. A portion of this stress is converted to heat and some other portions break the molecular bonds (which is one of the oil renewing reasons). Therefore, the film thickness is the main factor to analyze the behavior of lubricant and amount of losses and wears in gear meshing.

$$F_r = C_2 h_r B \tag{2.28}$$

Adapted gear contact film thickness calculated by the method of Hamrock and Dowson[23]:

$$h(X) = C_{11}[V_e(X)\eta_{M0}]^{0.67}[w(X)]^{-0.067}\left[R_{eq}(X)\right]^{0.464} \tag{2.29}$$

Since the lubricant pressure is zero in atmosphere pressure, the temperature-viscosity coefficient factor can be described as:

$$\delta = \frac{\ln \eta_{m0} - \ln \eta_m}{\theta - \theta_0} \tag{2.30}$$

Where θ is working temperature and subscript zero refers to ambient temperature. Rolling surface velocity is determinant in calculating the thermal loading factor that is the index of finding thermal reduction factor. Surface velocity is assumed to be half of rolling speed:

$$u = \frac{V_e(X)}{2} \tag{2.31}$$

Heat transfer through the lubricant film has reverse effect on the thermal deflection and better thermal conductivity of lubricants leads to less loss. For mineral oils that are being used in gear boxes the average value for thermal conductivity is 0.13W/m.K.

$$Q_m(X) = \frac{C_{12}\eta_{Mo}u^2\delta}{K_f} \tag{2.32}$$

Where δ is temperature-viscosity coefficient and K_f is thermal conductivity. With linearizing the graph of heat factor vs. thermal loading term, thermal factor can be defined as below:

$$\varphi_t(Q_m) = 0.5487\exp(-0.3088Q_m) + 0.443\exp(-0.012Q_m) \tag{2.33}$$

By multiplying oil film thickness and thermal factor to tooth effective width (B') the rolling resistive force will obtain. It is needed to mention that modifying tooth width is because of converting helical form of gear tooth to straight shape:

$$F_r(X) = C_2 h(X) \varphi_t(X) B' \tag{2.34}$$

$$B' = 1.26B - 8.375$$

Finally power losses due to rolling obtained by:

$$P_r = C_3 V_r(X) F_r(X) \tag{2.35}$$

2.5.3 Gliding losses

Gliding losses refers to friction losses due to skin contact between gearbox components. For instance, during gear shifting the operation of synchronizer that is based on friction is one of the gliding loss cases. Furthermore, in churning losses calculations (2.3.1) it is assumed that gears lateral gap is wide enough not to cause boundary layer blending and it means the contingency of gliding losses is zero.

In the case that external loads are affecting on gear train shaft axes, the clearance in bearings, packing and sealing components may let rotating surfaces touch each other and even scrape the housing skin. Nevertheless, since the light-duty vehicles are the matter of this study it can be assumed that the vehicle is supposed to run over plain roads most of the times, gliding losses can be neglected. Although in rapid accelerations and sudden breaks the difference on moment of inertia in transmission complex may cause some losses in this way, the total losses would not vary so much.

However, in other applications where the machine has more degree of freedom and relative acceleration (gravity) are exerted on the system, gliding losses must take into consideration as well as other losses.

2.5.4 Bearing Losses

In standard automobile gearboxes, helical gears are applied to provide a smoother power transfer and minimize the noise and vibration due to gear meshing, so in analyzing bearings

loads, lateral forces generated by helical tooth angle must considered for realistic results. Bearing losses mainly are dived into load dependent (M_L) and viscose torque (M_V) losses.

$$M = M_L + M_V \tag{2.36}$$

According to basic helical gear load distribution rules and Figure 2.10, since normal tooth load defined by w_n radial and axial loads are defined as below:

$$\left.\begin{aligned} F_A &= F_n \cos\alpha_n \, sin\,\beta \\ F_R &= F_n \sin\alpha_n \end{aligned}\right\} \tag{2.37}$$

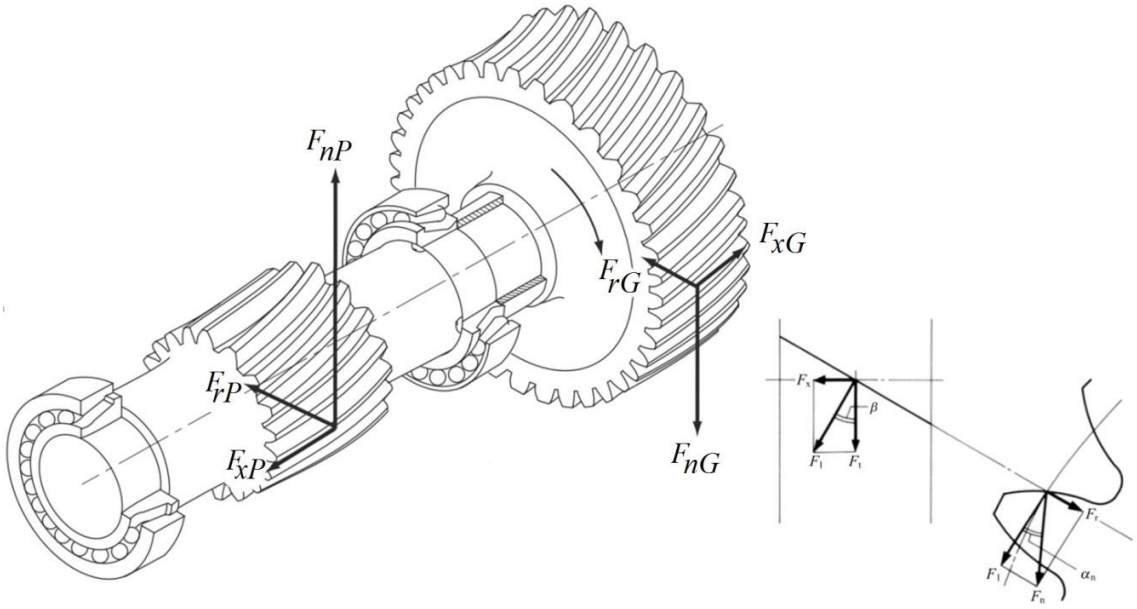

Figure 2.9. Forces acting on a helical gear mesh [25]

Regarding to Figure 2.9, F_A is the portion of tangential force applied on gear tooth deviated to thrust load on supporting bearings and radial load simply achieved by pressure angle. If normal tooth load defined as the function of time or displacement, it should be rewritten as blow:

$$\left.\begin{aligned} F_A &= w(X)\cos\alpha_n \sin\beta \\ F_R &= w(X)\sin\alpha_n \end{aligned}\right\} \quad (2.38)$$

Where β is tooth helix angle and α_n is pressure angle. According to ABEC methods and ABMA standards static equivalent load can be found by below relation:

$$F_{eq} = X_0 F_R + Y_0 F_A \quad (2.39)$$

Radial and thrust factors of bearings are read from bearing manufacturer catalogue. Bearing coefficient of friction is also available by providers which are between 0.001 and 0.003 depends on the type of roller component that can be spherical, cylindrical, needle etc. [29] Other geometries and characteristics of bearing mentioned in bearing catalogue. There are lots of different and vast studies about bearing losses with small differences is results that can be substituted with below equation but what is used in this work is experimentally improved and significantly more than proper enough for calculating total losses in the gearbox. [27]

$$M_L = 0.5 D_b F_{eq} \mu_b \quad (2.40)$$

Load dependent losses is a function of applied torque (M_L), bore diameter (D_b) and friction coefficient (μ_b). Therefore, by multiplying applied torque in rotational speed (n) the load dependent loss in bearing is:

$$P_{b,L} = 0.5 D_b F_{eq} \mu_b n \quad (2.41)$$

Another power loss sink in supporting bearings is thermal losses through frictional heat generation, which is a function of friction torque and rotational speed.

$$P_{b,th} = 1.05\,10^{-4} M_L n \tag{2.42}$$

Combining thermal and mechanical power losses will lead to total bearing load dependent power losses as below:

$$P_{b,L} = (1 + 1.05\,10^{-4}) M_L n \tag{2.43}$$

Load independent or viscose losses in bearings depend on lubricant viscosity since it changes relatively to temperature. Furthermore providing a precise general model from Newton's relation for viscose friction force $\tau = \boldsymbol{\rho}_{oil} C_d n^2$ is not straightforward in this case, so empirical formulas are used [27]:

$$P_{b,V} = M_V n$$

$$\left.\begin{aligned} M_V &= 10^{-7} \boldsymbol{f_L} {d_b}^3 (\nu_0 n)^{2/3} && \nu_0 n > 2000 \\ M_V &= 160\,10^{-7} \boldsymbol{f_L} {d_b}^3 && 2000 \leq \nu_0 n \end{aligned}\right\} \tag{2.44}$$

In above $\boldsymbol{f_L}$ represents the bearing lubricating condition that is findable from bearing catalogue [appendix E].

Finally, the total bearing losses due to bearings is the summation of individual bearings. However, it must be noticed that for calculation of effective load on each bearing, static and dynamic load distribution analysis needs to be done for all supports in free body mode, then separately for any sole bearing to find force vector component and defining the equivalent load on them.

2.6 Churning losses

In order to decrease the friction resistive force, lubricants are widely used to make the contact surfaces as slithery as possible. Even though adding lubricant to moving parts minimizes the resistive force, it causes some other resistances which are surcharging peripheral loads to the system. Despite of mechanical power losses in gear mating, the power losses due to fluid kinematic and dynamic characteristics is other compartment of total losses.

2.6.1 Oil Drag Power Losses

Gearbox interior is filled by a lubricant which is generally oil and depending on type of lubrication; fluid viscosity that develops oil film beneath clashing components also results in resistive forces. When a gear pair immerses to oil bath, the length of a chord that separates wetted and dry area on lateral gear/pinion surface is ℓ . The angle between vertical centerline and outer circle ray at intersection of circumference and oil level (r_o) illustrated by ϕ.

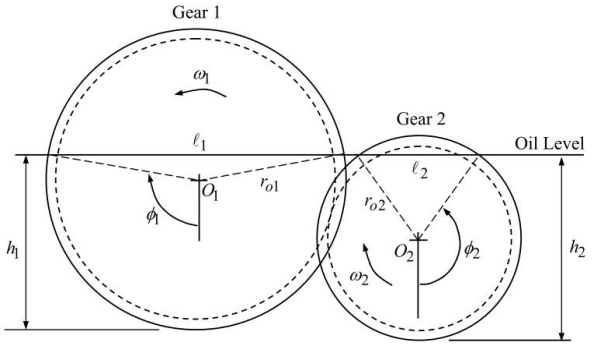

Figure 2.10. Definition of oil churning parameters for a gear pair immersed in oil[25].

Drag force is illustrating wherever a moving part entrains in between a fluid layers. In addition, according to the shape of part, speed and fluid viscosity, fluid adhesion resistance varies. In gearboxes, the portion of gears which are exposed to oil and air have different drag forces according to which fluid surrounds the gear periphery and face. Correspondingly, drag force mainly is divided to face (P_{df}) and periphery(P_{dp}):

$$P_d = P_{dp} + P_{df} \tag{2.45}$$

For periphery drag forces, first of all the portion of gear which is immersed in oil should be defined, and since gears are pivoting all the times there is no exact plain surface in oil bath, a mean value for constant height of oil is considered in equations. Regarding to Figure 2.10 this portion immersion mean value can be defined:

$$\bar{h} = \frac{h}{r_o} \tag{2.46}$$

Where $\bar{h}$ is immersion ratio and for $\bar{h} \geq 2$ it means that gear is completely drawn in oil and for zero values of $\bar{h}$ gear is totally out of oil bath. By solving Navier-Stokes equations of motion for polar coordination with boundless circumference assumption, it indicates that only remaining shear stress is tangential shear stress which is $\tau = 2\omega\eta_M$. It should be mentioned that it is assumed that there is no interference among boundary layers along different gear, it means there is enough space between gears that independent boundary layer can develop over each gear periphery. So for calculating the oil drag:

$$F_{dp} = \frac{1}{2}\boldsymbol{\rho}_{\mathrm{eq}} U^2 A_{dp} C_{dp} \tag{2.47}$$

Where $\boldsymbol{\rho}_{\mathrm{eq}}$ is the combined fluid density. The gear spinning causes foaming then a mixture of oil and air is in contact with gears, which has different density from lubricant. Equivalent viscosity of fluid also changes in result of foaming and it is a combination of lubricant and air viscosity. According to Anderson and Loewenthal's report the equivalent density and viscosity is:

$$\left.\begin{aligned}\boldsymbol{\rho}_{eq} &= \frac{\boldsymbol{\rho}_{oil} + 34.35\boldsymbol{\rho}_{air}}{35.25} \\ \eta_{m,eq} &= \frac{\eta_{m,oil} + 34.35\eta_{m,air}}{35.25}\end{aligned}\right\} \quad (2.48)$$

U is linear velocity and C_{dp} is drag coefficient. A_{dp} is the wetted area on both lateral side of gear which is equal to $2r_o\phi b$ and $\phi = \cos^{-1}(1-\bar{h})$. Oil drag coefficient is defined as below:

$$C_{dp} = \frac{2\tau}{\rho_{eq}U^2} \quad (2.49)$$

By embedding C_{dp} and A_{dp} in equation (2.40) and substituting $U = r_o\omega$ final peripheral drag power losses is derive as:

$$P_{dp} = 4\eta_m {r_o}^2 \omega^2 \phi \quad (2.50)$$

Since gear speed variation is high in vehicle transmission for gear facial drag modeling, the current flow regime must be taken into consideration, so laminar and turbulent flows should be studied separately. For calculating boundary layer thickness and separation point on gear face there are to possible methods; flow near to rotating disc and flow over a wall. When gear is totally running in air or submerged in oil, rotary disc model is the proper choice but while gears are partially contaminated with oil and relative immersion is happening in the system, flow over a wall is more convenient in this case.

Non-slip boundary layer assumption and large speed gradient from inner and outer points on gear surface, necessitates categorizing flow regime in to laminar, transient and turbulent flow according to Reynolds number within the range 10^5 to 10^6. The Reynolds number for gear surface can be defined as below: [26]

$$R_e = \frac{2\rho\omega {r_o}^2}{\eta_m} \tag{2.51}$$

- **Laminar flow regime**

Velocity profile below boundary layer is assumed to be linear and related to how far is from surface. Maximum length of boundary layer happens when gear completely submerged. Again by solving boundary layer thickness and facial drag coefficient equations, the drag force on gear face will be:

$$F_{df}^{L} = \frac{1}{2}\rho_{\text{eq}} U^2 A_{df} C_{df}^{L} \tag{2.52}$$

Where gear wetted face area calculation is:

$$A_{df} = {r_o}^2\left[\frac{\pi}{2} - sin^{-1}(1-\bar{h}) - (1-\bar{h})\sqrt{\bar{h}(2-\bar{h})}\right] \tag{2.53}$$

In addition, laminar drag coefficient for gear face derived:

$$C_{df}^{L} = 0.578\sqrt{\frac{\nu_0}{\ell\, U}} \tag{2.54}$$

Term ℓ defined as $2r_0 \sin\phi$. Gear face drag resistance force calculated for one side of gear and by this assumption that gear is in a symmetric condition along its axis, facial drag power losses for laminar flow can obtained by multiplying drag force with fact 2 and speed. By substituting linear speed by rotational terms $r_0\omega$:

$$P_{df}^{L} = \rho(r_0\omega)^3 A_{df} C_{df}^{L} \tag{2.55}$$

For the case that the gear, which is fully submerged in lubricant ($\bar{h} = 2$), above equation can be simplified in below format:

$$P_{df}^{L} = \frac{0.41\boldsymbol{\rho}_{eq}{\nu_0}^{0.5}{r_0}^{2}\omega^{2.5}A_{df}}{\sqrt{sin\,\phi}} \tag{2.56}$$

- **Turbulent flow regime**

Same assumptions are applied in turbulent flow analysis on the gear face and using Prandtl law [26] for plain surface, speed profile will be the ratio of seventh root of perpendicular distance on boundary layer thickness multiplied by gear speed. Solving boundary layer equation leads to define surface drag coefficient for turbulent regime:

$$C_{df}^{T} = 0.0276[\frac{\nu_0}{\ell U}]^{1/7} \tag{2.57}$$

Main principle of flow drag forces is utilized for turbulent regime and same wetted surface carries drag load. Equivalent density and kinematic viscosity in turbulent flow is different from laminar flow and correspondingly varies the boundary layer thickness and drag coefficient but it is negligible comparing to the total power losses whilst the equivalent value for density and viscosity is almost the same as laminar flow.

$$F_{df}^{T} = \frac{1}{2}\boldsymbol{\rho}_{\mathrm{eq}}U^{2}A_{df}C_{df}^{T} \tag{2.58}$$

By substituting main formula elements by geometric parameters, facial drag force in turbulent regime can be rewritten as:

$$F_{df}^{T} = \frac{0.025\boldsymbol{\rho}_{\mathrm{eq}}{\nu_0}^{0.143}{r_0}^{1.714}\omega^{1.857}A_{df}}{(sin\,\phi)^{0.143}} \tag{2.59}$$

Finally gathering all terms and adding speed to resistive drag force with simplifications leads to general equation for turbulent flow, lateral drag power losses in gear:

$$P_{df}^{T} = \frac{0.025\boldsymbol{\rho}_{\mathrm{eq}}\nu_0^{0.143} r_0^{2.714}\omega^{2.857}A_{df}}{(\sin\phi)^{0.143}} \tag{2.60}$$

2.6.2 Power Losses due to root filling

Depending on immersion ratio, cavities in between of neighbor teeth are filled by oil when the gear teeth plunge into the oil bath and carry an amount of volume of oil with them. This volume assumed to be a controlled volume to utilize Navier-Stokes and stream function $\psi(r,\theta)$ in polar coordination. The fluid swirling through the cavity edges is modeled by the sidewall flow, so the accelerated oil in cavities leads to eddy flows that are not in the same direction as oil flow direction and this causes in energy waste and loss in power. In this model the gear is assumed stationary while a creeping flow of incompressible viscose fluid swirling past the adjacent teeth cavity.

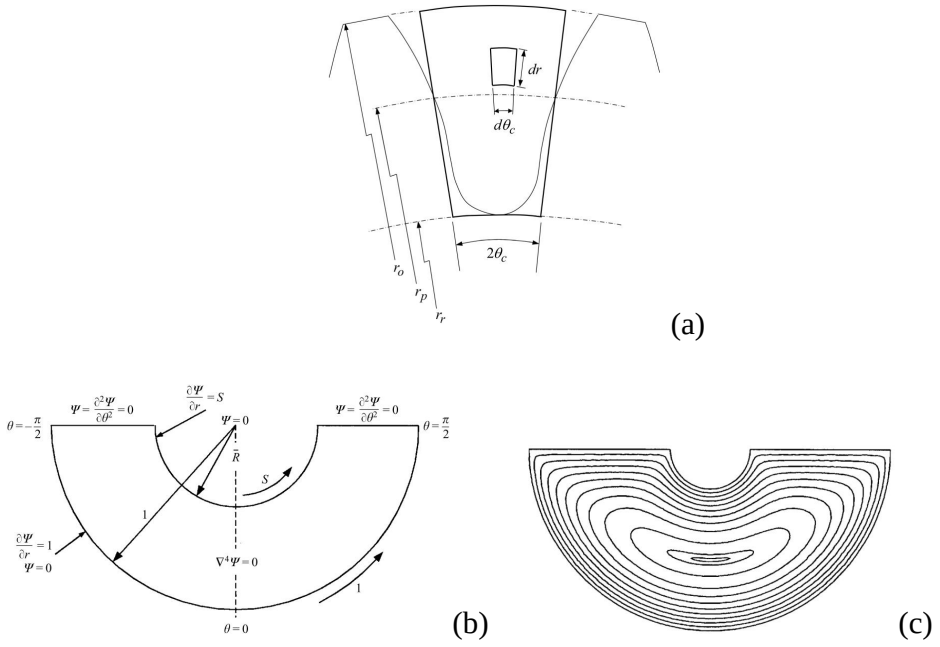

Figure 2.11. Geometric parameters associated with root filling power losses [28]

Defining the controlled volume for tooth cavity is not easy while the involute cross section of gear is hard to define in an analytical way. What is assumed as cross section area of gear tooth is defined in Figure 2.11.

While the relative speed of flow in cavities is slow, so in Navier-Stokes equation second power of speed can be neglected. Denoting the boundary condition in gear teeth cavity (a) is different from half circle annual flow and restricted to $\pm\theta_c$ instead of $\pm\frac{\pi}{2}$ (b) and equipotential curves are assumed to be concentric with gear pitch circle so $u_r = \frac{1}{r}\frac{\partial\psi}{\partial\theta} = 0$ (c).

Bi-harmonic two-dimensional equation for creeping type of radial flow around boundaries due to tangential velocity derives as below:

$$\nabla^4\psi = \frac{d^4\psi}{dr^4} + \frac{2d^3\psi}{rdr^3} - \frac{d^2\psi}{r^2dr^3} + \frac{d\psi}{r^3dr} = 0 \tag{2.61}$$

Indicating above equations, angular gradient of flow function is assumed to be zero, flow is steady Stoke type, only radial effect of eddies considered and gravity is neglected. So stream function is dependent on radial variation only $\psi(r,\theta) = \psi(r)$. Solving differential equation (2.61) respecting to variable (r):

$$\psi = D_1 + D_2r^2 + D_3 \log r + D_4r^2 \log r \tag{2.62}$$

Defining boundary condition for gear annular cavity:

$$\psi = \begin{cases} 0 \;\; at \;\; r = r_o \;\;\; |\theta| \le \theta_c \\ 0 \;\; at \;\; r = r_r \;\;\; |\theta| \ge \theta_c \end{cases} \tag{2.63}$$

Moreover, for radial derivation:

$$\frac{d\psi}{dr} = \begin{cases} -\omega r_o \;\; at \;\; r = r_o \;\;\; |\theta| \leq \theta_c \\ -\omega r_r \;\; at \;\; r = r_r \;\;\; |\theta| \leq \theta_c \end{cases} \tag{2.64}$$

Where r_o is outer radius, r_r is tooth root radius and $2\theta_c$ is cavity angle at pitch radius (r_p). Applying boundary condition in equation (2.62) will result in four equations, four unknown that gives the coefficients (D):

$$\begin{cases} D_1 + D_2 r_o^2 + D_3 \log r_o + D_4 r_o^2 \log r_o = 0 \\ 2D_2 r_o + \dfrac{1}{r_o} D_3 + r_o(1 + 2\log r_o) D_4 = -\omega r_o \\ D_1 + D_2 r_r^2 + D_3 \log r_r + D_4 r_r^2 \log r = 0 \\ 2D_2 r_r + \dfrac{1}{r_o} D_3 + r_r(1 + 2\log r_r) D_4 = -\omega r_r \end{cases} \tag{2.65}$$

By extracting coefficients from above equation, tangential velocity in steady stream is:

$$u_r = -\frac{\partial \psi}{\partial r} = -[2D_2 r + \frac{D_3}{r} + D_4 r + 2D_4 r \log r] \tag{2.66}$$

Tangential shear stress on cavities face will be:

$$\tau_f = \eta_m r \frac{\partial}{\partial r}\left(\frac{u_r}{r}\right) = 2\eta_m (\frac{D_3}{r^2} - \frac{D_4}{r}) \tag{2.67}$$

The reciprocating force between in the cavity face and fluid due to shear stress will obtain:

$$F_f(r\theta) = A_c \tau_f = 2\eta_m A_c (\frac{D_3}{r^2} - D_4) \tag{2.68}$$

Where $A_c = (r_o^2 - r_r^2)\left(\frac{2\theta_c}{\pi}\right)$ is cavity cross section area from Figure 2.11 (a). The amount of dissipated torque for fluid swirling among gear cavities is:

$$T_f = \int_{r_r}^{r_o} F_f(r,\theta)\, dr = 2\eta_{m,eq} A_c (r_o - r_r)[\frac{D_3}{r_o r_r} - D_4] \quad (2.69)$$

Finally the power losses due to root filling for a single cavity can be calculated by applying angular speed and depending on immersion ratio the number of acting teeth, N, should multiply by the power loss equation:

$$P_f = 2N\eta_m A_c (r_o - r_r)\omega[\frac{D_3}{r_o r_r} - D_4] \quad (2.70)$$

Root filling power losses need to be calculated for any gear separately then total loss would be the summation of them $P_f = \sum P_{fi}$.

2.6.3 Oil Pocketing Power Losses

The cavity between two adjacent teeth partially fills by the opponent gear teeth during mesh cycle. The trapped oil in between teeth clearance will squeezed then and thrown away in lateral direction. This phenomenon is similar to oil circulation in geared oil pumps. The volume of trapped oil mainly can be divided in to three regions as shown in Figure 2.12. In order to apply continuity equations for calculating the amount demanded force and power to pump-out the trapped oil, control H_{ij}^mvolume assumed for this section also, oil pocketing that happens during mesh cycle discretized in 3 sequences.

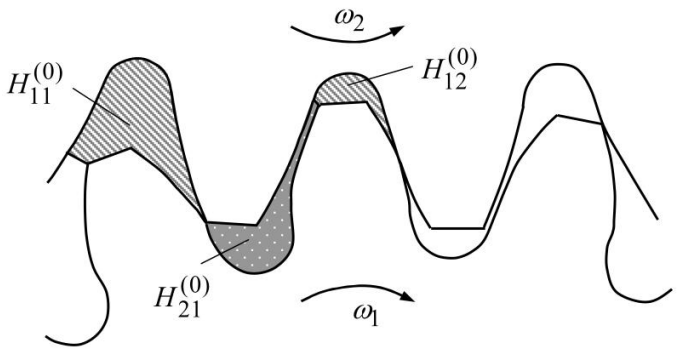

Figure 2.12. Illustration of a side view of fluid control volumes of the gear mesh interface

Generally, in this system it is considered that control volume is squeezed while carried by teeth. Then by parametric defining of control volume as function of rotation angle, it can be calculated in each sequence. Applying Bernoulli's principle helps to find backlash and end flow pressure. Then according to conservation of momentum principle, lateral and backlash power losses can be calculated. [25, 26]

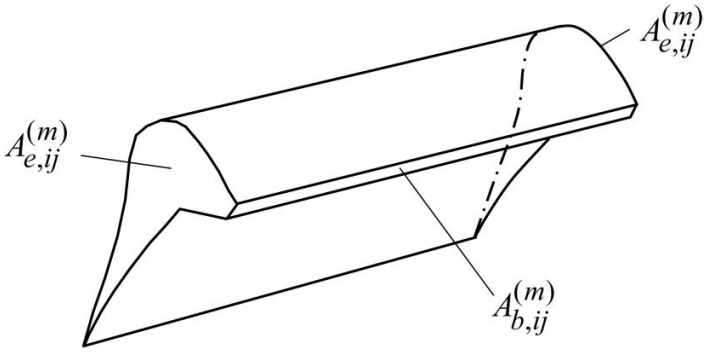

Figure 2.13. perspective of a control volume showing backlash and end flow areas

Massive analytical and trigonometric calculations are done to find a general solution for defining backlash volume in an arbitrary position of teeth that tried to explain briefly. The main idea and method adopted from Satya Seetharaman's dissertation (chapter 2.5) [25] and correspondingly its references so for information and mathematical manipulation that is more detailed, it suggested to refer to Satya Seetharaman's dissertation.

Schematic perspective of controlled volume is illustrated in Figure 2.13 that superscript m refers to sequence number and is dependent to rotation angle from start of tooth engagement. Subscript ‘b’ and ‘e’ are representing backlash and end flow area. In order to calculate the end flow area $\mathsf{A}_{\mathrm{e,ij}}^{(\mathrm{m})}$ and backlash area $\mathsf{A}_{\mathrm{b,ij}}^{(\mathrm{m})}$ in accordance of gears and mating geometries, whole of cavity between adjacent teeth is divided in to four divisions in Figure 2.14:

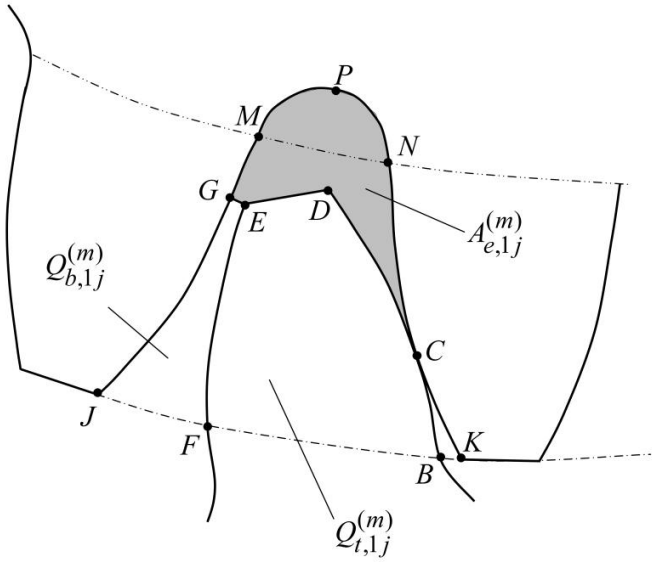

Figure 2.14. Definition of the end area at an arbitrary position m .

In order to calculate $\mathsf{A}_{\mathrm{e,ij}}^{(\mathrm{m})}$ and $\mathsf{A}_{\mathrm{b,ij}}^{(\mathrm{m})}$, where subscript (i) refers to any arbitrary realvant gear mesh control volume and subscript (j) refers to which gear is in contact. Many geometrical terms have to be defined. For having a continuously functioning model and slight computer solvable algorithm, some assumptions and compromises were unavoidable. Geometries and variables in further equations are shown in Figure 2.15, where subscript 1 refers to driving pinion and subscript 2 refers to driven gear. Point B is start of active profile (SAP) which is the intersection of the limit diameter and the involute profile of gear 1 and the distance between O_1 and B at first stage is r_{s1}. Furthermore, the contour above CE is the control volume lateral area. Point E is tooth tip corner and $EO_1$is equal to outer diameter of gear 1 (r_{o1}). $O_1$and O_2 are gear pair centers. In the below figure, gears seem to be symmetric but it should be noticed that, generally they have different dimensions and geometries. Term e is

distance between centers. Parameters in Figure 2.15 have superscript *m*, which indicates the frame number of one tooth action from beginning to end. At the first moment, that driving tooth touches the driven gear tooth *m=0* and when driver tooth leaves its pair *m=M.*

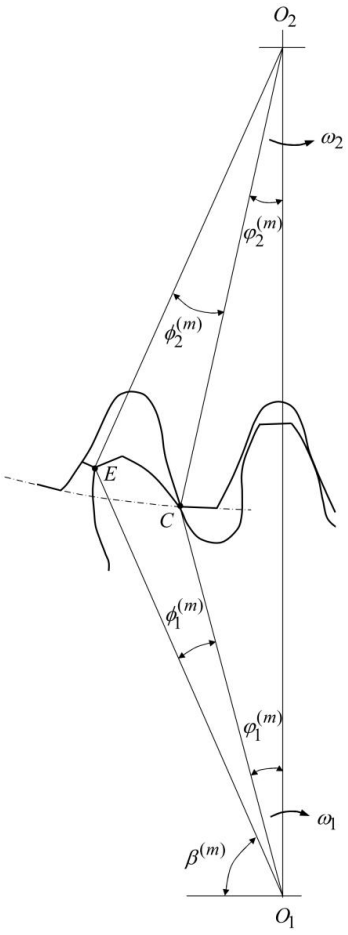

Figure 2.15. Geometry of two gears in mesh at an arbitrary position m.

As mentioned above control volume will be a function of gear rotation, so rotating angle increases from $\theta_{i0} = [\frac{r_{si}^2}{r_{bi}^2} - 1]^{1/2}$ by rate of *m/M* in $\overline{\theta_i} = [\frac{r_{oi}^2}{r_{bi}^2} - 1]^{1/2} - [\frac{r_{si}^2}{r_{bi}^2} - 1]^{1/2}$ .The incremental angle is given as:

$$\theta_{im} = \theta_{i0} + \frac{m}{M}\overline{\theta_i} \tag{2.71}$$

Angles in Figure 2.15 are defined in below by means of geometric analysis and trigonometric functions at the beginnig of action where *m=0*:

$$\varphi_1^{(0)} = \cos^{-1}[\frac{e^2 + r_{s1}^2 - r_{o2}^2}{2er_{s1}}] \quad (2.72)$$

$$\varphi_2^{(0)} = \cos^{-1}[\frac{e^2 + r_{o2}^2 - r_{s1}^2}{2er_{o2}}]$$

$$\phi_1^{(0)} = (\frac{r_{o1}^2}{r_{b1}^2} - 1)^{1/2} - \cos^{-1}[\frac{r_{b1}}{r_{o1}}] - (\frac{r_{s1}^2}{r_{b1}^2} - 1)^{1/2} + \cos^{-1}[\frac{r_{b1}}{r_{s1}}] + \frac{DE}{r_{o1}}$$

$$\phi_2^{(0)} = \cos^{-1}[\frac{e^2 + (O_2E^{(0)})^2 - r_{o1}^2}{2eO_2E^{(0)}}] - \varphi_2^{(0)}$$

$$\beta^{(0)} = \frac{\pi}{2} - (\varphi_1^{(0)} + \phi_1^{(0)})$$

Where e is the distance between gaer and pinion centers, r_{b1} is base radius of gear 1 and *DE* is tooth thickness of gear 1at the tip. Assuming the same tooth tip thickness for both gears, and since the tooth tip thickness compard to r_{o2} is small enough to assume: $\sin(DO_2E) \cong DO_2E$, then angles $CO_2J^{(0)} = (\frac{2\pi}{n_2} - \frac{DE}{r_{o2}})$ and $CO_2G^{(0)} = CO_2J^{(0)} - JO_2G^{(0)}$ can be defined and by virtual coencidencity of point E and G ($O_2E^{(0)} \approx O_2G^{(0)}$) then according to vectors sum rule, below relations can be derived:

$$CO_2J^{(0)} = \frac{2\pi}{N_2} - \frac{DE}{r_{o2}} \quad (2.73)$$

$$O_2E^{(0)} = \sqrt{e^2 + r_{o1}^2 - 2er_{o1}\sin[\beta^{(0)}]}$$

$$JO_2G^{(0)} = (\frac{r_{o2}^2}{r_{b2}^2} - 1)^{1/2} - \cos^{-1}[\frac{r_{b2}}{r_{o2}}] - [(\frac{O_2E^{(0)}}{r_{o2}})^2 - 1]^{1/2} + \cos^{-1}[\frac{r_{b2}}{O_2E^{(0)}}]$$

Again assuming small angles, the backlash length $EG^{(0)}$ can be expressed as its radius multiplied by the angle $EG^{(0)} = O_2E^{(0)}.EO_2G^{(0)}$. For calculating backlash angle there other ways available and it also can be read from gear catalogue, but according to above

figures it is defined as $EO_2G^{(0)} = CO_2J^{(0)} - JO_2G^{(0)} - \phi_2^{(0)}$. Hence, the backlash flow area for the first control volume ($H_{11}^{(0)}$) at initial position is derived as:

$$A_{b,11}^{(0)} = b\,\overline{EG}^{(0)} \tag{2.74}$$

Where b is effective face width of gear tooth contact.

The backlash flow area which is calculated above is for first frame, in order to have a general equation for an arbitrary position, it is needed to modify the angles and geometries before and after pitch point.

$$\begin{aligned}
&\beta^{(m)} = \beta^{(0)} + (m-1)\Delta\theta_{1m} \\
&\phi_1^{(m)} = \frac{DE}{r_{o1}} + \left(\frac{r_{o1}^2}{r_{b1}^2} - 1\right)^{1/2} - \cos^{-1}\left[\frac{r_{b1}}{r_{o1}}\right] - \left[\left(\frac{O_1C^{(m)}}{r_{b1}}\right)^2 - 1\right]^{1/2} + \cos^{-1}\left[\frac{r_{b1}}{O_1C^{(m)}}\right] \\
&\varphi_1^{(m)} = \begin{cases} \frac{\pi}{2} - (\beta^{(m)} + \phi_1^{(m)}) & \beta^{(m)} \le \frac{\pi}{2} \\ (\beta^{(m)} + \phi_1^{(m)}) - \frac{\pi}{2} & \beta^{(m)} \ge \frac{\pi}{2} \end{cases} \\
&\varphi_2^{(m)} = \sin^{-1}\left[\frac{O_1C^{(m)}\sin(\varphi_1^{(m)})}{O_2C^{(m)}}\right] \\
&\phi_2^{(m)} = \sin^{-1}\left[\frac{r_{o1}\sin\left(\phi_1^{(m)} + \varphi_1^{(m)}\right)}{O_2E^{(m)}}\right] - \varphi_2^{(m)}
\end{aligned} \tag{2.75}$$

Since *C* moving on line of action all the times $O_1C^{(m)} = r_p\,cos\varphi_1^{(m)}$, the length between center of gear 2 and tip point og gear 1 is $O_2E^{(m)} = \sqrt{e^2 + r_{o1}^2 - 2er_{o1}\cos(\phi_1^{(m)} + \varphi_1^{(m)})}$ and distance between contact point and center of gear2 is $O_2C^{(m)} = \sqrt{e^2 + (O_1C^{(m)})^2 - 2eO_1C^{(m)}\cos(\varphi_1^{(m)})}$.

Since point J is fixed, its radius in gear 2 can be shown as r_{o2} and regarding to Figure 2.16 angle $CO_2G^{(m)} = CO_2J^{(m)} - JO_2G^{(m)}$. By a rough assumption of $O_2G^{(0)} \approx O_2E^{(0)}$ following equations are:

$$CO_2J^{(m)} = CO_2J^{(0)} - (\frac{r_{o2}^2}{r_{b2}^2} - 1)^{1/2} - \cos^{-1}[\frac{r_{b2}}{r_{o2}}] + [(\frac{O_2C^{(m)}}{r_{b1}})^2 - 1]^{1/2} + \cos(\frac{r_{b2}}{O_2E^{(0)}}) \quad (2.76)$$

$$JO_2G^{(m)} = (\frac{r_{o2}^2}{r_{b2}^2} - 1)^{1/2} - \cos^{-1}[\frac{r_{b2}}{r_{o2}}] - [(\frac{O_2E^{(m)}}{r_{o2}})^2 - 1]^{1/2} + \cos^{-1}[\frac{r_{b2}}{O_2E^{(m)}}]$$

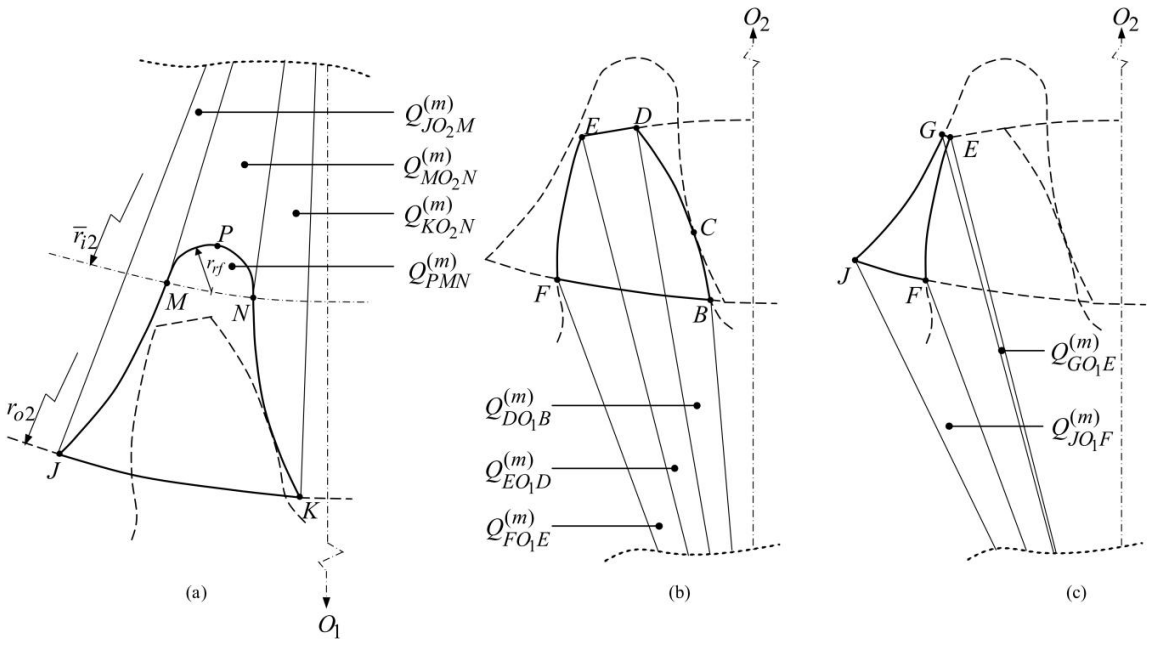

Figure 2.16. Parameters used in calculation of (a) the total tooth cavity area Q_{c2}, (b)the overlap area $Q_{t,1j}^{(m)}$ and (c) the excluded area $Q_{b,1j}^{(m)}$

For calculating the tangential backlash length on angle of $EG^{(m)}$, with above assumptions, $EG^{(m)} = O_2E^{(m)}.EO_2G^{(m)}$ where:

$$EO_2G^{(m)} = CO_2J^{(m)} - (JO_2G^{(m)} + \phi_2^{(m)}) \tag{2.77}$$

Finally the backlash flow area in any position coresponding to *m*, for control volume $H_{11}^{(m)}$ can be defined as below:

$$A_{b,11}^{(m)} = b\, EG^{(m)} \tag{2.78}$$

Where, the same as initial condition, b is effective gear width.

Calculation of all control volumes leads to a full variation of backlash areas during mesh cycle. Since the provided model is based on gear geometries, for $\mathrm{H}_{12}^{(\mathrm{m})}$ the same way can be applied to determine the $\mathrm{A}_{\mathrm{b,ij}}^{(\mathrm{m})}$ for each gear at any sequence.

In order to fully define the control volume borders, end flow area also should be calculated. According to Figure 2.16:

$$A_{e,1j}^{(m)} = Q_{c2} - [Q_{t,1j}^{(m)} + Q_{b,1j}^{(m)} + Q_{BCK}^{(m)}] \tag{2.79}$$

Where Q_{c2} is total cavity lateral surface and what is in bracket in equation (2.79) is the overlapped areas, so by subtracting overlapped surfaces, desired end flow area will achieved. Relative geometries and analytical calculation briefly explained in this chapter and for detailed understanding of mathematical process it refers to study reference. [28] Areas illustrated in Figure 2.16 will calculate step by step and finally net end flow area will be obtained. Area $Q_{BCK}^{(m)}$ at beginnig of action period is zero and whilst is an expanding area may have sucking effect on oil which is not considered in this study; thus, its effect comparing to Q_{c2} in negligible.

- **Calculation of Area Q_{c2}**

For this area, first the sector of full gear face that belonged to each tooth is calculated, then redundant areas are extracted:

$$Q_{c2} = Q_{JO_2K} - [Q_{JO_2M} + Q_{KO_2N} + (Q_{NO_2M} - Q_{PMN})] \tag{2.80}$$

Assuming circular profile of a symmetric involut gear tooth the cavity area can be achieved:

$$Q_{c2} = \frac{1}{2} r_{o2} \left(\frac{2\pi r_{o2}}{N_2} - T_{o2} \right) - 2 \iint_{JO_2M} I_{JM}(\theta) dr d\theta - \frac{1}{2} r_{b2} \left(\frac{2\pi r_{b2}}{N_2} - T_{b2} \right) + \frac{1}{2} \pi r_{rf2} \tag{2.81}$$

Where I_{JM} is involute profile radius, T_{o2} and T_{b2} are circular tooth thicknesses at the tip and base circle. Involute profile function as function of θ can be expressed in simple version of $I_{JM} = \sqrt{r_{b2} + [1 + (3\theta)^{2/3}]}$ and by converting the function in Taylor series form, the first three terms of Taylor expansion polynomial of double integration on surface will be:

$$\iint_{JO_2M} I_{JM}(\theta) dr d\theta = \frac{1}{2} r_{b2} [(\theta_M - \theta_J) + 0.46(\theta_M^{2.33} - \theta_J^{2.33}) + 1.25(\theta_M^{1.67} - \theta_J^{1.67})] \tag{2.82}$$

Where θ_M and θ_J are the horizontal angles of O_2M and O_2J from XO_2. By substituting equation (2.82) into (2.81) value of Q_{c2} will obtained.

- **Calculation of Area $Q_{t,1j}^{(m)}$**

Calculating penetrated tooth of gear 1 into cavity of gear 2 is done by below equaion:

$$Q_{t,1j}^{(m)} = \left({Q_{DO_1B}}^m + Q_{EO_1D} + {Q_{FO_1E}}^m \right) - {Q_{FO_1B}}^m \tag{2.83}$$

According to Figure 2.16 with same assumptions in calculating area Q_{c2}:

$$Q_{t,1j}^{(m)} = \iint_{DO_1B} I_{BD}(\theta)drd\theta + \frac{1}{2}r_{O1}T_{O1} + \iint_{FO_1E} I_{FE}(\theta)drd\theta - \iint_{FO_1B} I_{BF}(\theta)drd\theta \quad (2.84)$$

Where $I_{BD}(\theta)$ and $I_{FE}(\theta)$ both approximated by $I(\theta) = r_{b1}[1 + 0.5(3\theta^{2/3})]$, so the corresponding integration of drive edge profile functions are:

(2.85)

$$\iint_{BO_1D} I_{BD}(\theta)drd\theta = \frac{1}{2}r_{b1}^2[(\theta_B - \theta_D) + 0.46\{(\theta_R - \theta_D)^{2.33} - (\theta_R - \theta_B)^{2.33}\} + 1.25\{(\theta_R - \theta_D)^{1.67} - (\theta_R - \theta_B)^{1.67}\}$$

$$\iint_{FO_1E} I_{FE}(\theta)drd\theta = \frac{1}{2}r_{b1}^2[(\theta_E - \theta_F) + 0.46\{(\theta_E - \theta_Q)^{2.33} - (\theta_F - \theta_Q)^{2.33}\} + 1.25\{(\theta_E - \theta_Q)^{1.67} - (\theta_F - \theta_Q)^{1.67}\}$$

Where θ_B, θ_D, θ_E and θ_F are angles made by intersection of O_1B, O_1D, O_1E and O_1F with horizontal center line of gear1, XO_1. And θ_Q is rotating angle of gear1. For evaluating the third term of Eq. (2.48), I_{BF} initialized by $I_{BF}(\theta) = e\sin\theta - \sqrt{r_{o2}^2 - e^2\sin^2\theta}$, thus last integration is:

$$\iint_{BO_1F} I_{BF}(\theta)drd\theta = \frac{1}{2}r_{o2}^2[(\theta_B - \theta_F) + \frac{1}{4}e^2[\sin(2\theta_B) - \sin(2\theta_F)] + \frac{1}{2}r_{o2}^2[\sin^{-1}(\frac{e\cos\theta_B}{r_{o2}}) - \sin^{-1}(\frac{e\cos\theta_F}{r_{o2}})] + \frac{1}{2}er_{o2}[\cos\theta_B\sqrt{1 - (\frac{e\cos\theta_B}{r_{o2}})^2} - \cos\theta_F\sqrt{1 - (\frac{e\cos\theta_F}{r_{O2}})^2}] \quad (2.86)$$

- **Calculation of Area $Q_{b,1j}^{(m)}$**

Extracting the trailing area by below equation:

$$Q_{b,1j}^{(m)} = \left(Q_{GO_1E}^{(m)} + Q_{JO_1G}^{(m)}\right) - (Q_{JO_1F}^{(m)} + Q_{FO_1E}^{(m)}) \tag{2.87}$$

In order to calculate the area of ${Q_{GO_1E}}^{m}$, a new variable s is needed to be defined by $s = \frac{1}{2}(EG^m + O_1E^m + O_1G^m)$, then:

$$Q_{GO_1E}^{(m)} = s\sqrt{(s - EG^{(m)})(s - O_1E^{(m)})(s - O_1G^{(m)})} \tag{2.88}$$

The other areas will be calculated by double integration on surface:

$$Q_{b,1j}^{(m)} = Q_{GO_1E}^{(m)} + \iint_{JO_1G} I_{JG}(\theta)drd\theta - \iint_{JO_1F} I_{JF}(\theta)drd\theta - \iint_{FO_1E} I_{FE}(\theta)drd\theta \tag{2.89}$$

Last term of above equation ($\iint_{FO_1E} I_{FE}(\theta)drd\theta$) is calculated in Eq. (2.85). Given $I_{JF}(\theta) = e\sin\theta - \sqrt{r_{o2}^2 - e^2\sin^2\theta}$ and $I_{JG}(\theta) = e\sin\theta - \sqrt{r_{inv}^2 - e^2\sin^2\theta}$ for $Q_{JO_1F}^{(m)}$ an $Q_{JO_1G}^{(m)}$ will lead to:

$$\iint_{JO_1F} I_{JF}(\theta)drd\theta = \frac{1}{2}r_{o2}^2(\theta_F - \theta_J) - \frac{1}{4}e^2[\sin(2\theta_F) - \sin(2\theta_J)] \tag{2.90}$$
$$+\frac{1}{2}r_{o2}^2[\sin^{-1}(\frac{e\cos\theta_F}{r_{o2}}) - \sin^{-1}(\frac{e\cos\theta_J}{r_{O2}})]$$
$$+\frac{1}{2}er_{o2}[\cos\theta_F\sqrt{1-(\frac{e\cos\theta_F}{r_{o2}})^2} - \cos\theta_J\sqrt{1-(\frac{e\cos\theta_J}{r_{o2}})^2}]$$

$$\iint_{JO_1G} I_{JG}(\theta)drd\theta = \frac{1}{2}r_{inv}^2(\theta_G - \theta_J) - \frac{1}{4}e^2[\sin(2\theta_G) - \sin(2\theta_J)]$$
$$+\frac{1}{2}r_{inv}^2[\sin^{-1}(\frac{e\cos\theta_G}{r_{o2}}) - \sin^{-1}(\frac{e\cos\theta_J}{r_{O2}})]$$
$$+\frac{1}{2}er_{inv}[\cos\theta_G\sqrt{1-(\frac{e\cos\theta_G}{r_{o2}})^2} - \cos\theta_J\sqrt{1-(\frac{e\cos\theta_J}{r_{o2}})^2}]$$

Where r_{inv} is the distance between driver gear center to back step driven tooth involute curve that varies from O_1J to O_1G by rotaion of gears. It can be expressed as RMS value of O_1J to O_1G.

According to the empirical tests, end flow area can be defined as function of rotation and initial cavity cross section:

$$A_{e,ij} = \frac{2\cot\beta^{(m)} + 0.2}{A_{c,ij}} \tag{2.91}$$

Now having the backlash and end flow area and utilizing the integral form of the continuity equation: [26]

$$\frac{d}{dt}\int_V \boldsymbol{\rho} dV = -\oint_S \boldsymbol{\rho} v.\mathbf{n} dS \tag{2.92}$$

Where V is arbitrary volume, υ is flow speed and **n** is surface normal vecto. Assuming one direction flow in each surface, compromising three dimensional speed vector by defining $\zeta^{(m)} = A_{b,ij}^{(m)}/(2A_{e,ij}^{(m)} + A_{b,ij}^{(m)})$ with one direction speed to simplify the computations and

considering decreasing volume while oil is pumped out of gear teeth clearance. The outgoing speed of oil through cavity from back and surface as function of control volume variations is derived as:

$$\upsilon_{b,ij}^{(m)} = \frac{\zeta^{(m)}}{A_{b,ij}^{(m)}} \frac{dV_{ij}^{(m)}}{d\theta} \omega_i \tag{2.93}$$

$$\upsilon_{e,ij}^{(m)} = \frac{(1-\zeta^{(m)})}{A_{e,ij}^{(m)}} \frac{dV_{ij}^{(m)}}{d\theta} \omega_i$$

Following Bernoulli's principle for pressure gradient in control volume H_{ij}^{m} will result in:

$$\mathbf{P}_{b,ij}^{(m)} = P_{b,ij}^{(m-1)} + \frac{1}{2}\boldsymbol{\rho}[(\upsilon_{b,ij}^{(m-1)})^2 - (\upsilon_{b,ij}^{(m)})^2] \tag{2.94}$$

$$\mathbf{P}_{e,ij}^{(m)} = P_{e,ij}^{(m-1)} + \frac{1}{2}\boldsymbol{\rho}[(\upsilon_{e,ij}^{(m-1)})^2 - (\upsilon_{e,ij}^{(m)})^2]$$

And corresponding force on defined surfaces assuming pressure contributed evenly and it is independent of area elements:

$$F_{b,ij}^{(m)} = -\int_S P_{b,ij}^{(m)}\, dA_{b,ij}^{(m)} = -P_{b,ij}^{(m)} A_{b,ij}^{(m)} \tag{2.95}$$

$$F_{e,ij}^{(m)} = -\int_S P_{e,ij}^{(m)}\, dA_{e,ij}^{(m)} = -P_{e,ij}^{(m)} A_{b,ij}^{(m)}$$

Wher F_b and F_e are bakclash and end flow hydrualyc force. The power losses due to oil pocketing, considering bilateral exiting surface will be obtained as below:

$$P_{p,ij}^{(m)} = \upsilon_{b,ij}^{(m)} F_{b,ij}^{(m)} + 2\upsilon_{e,ij}^{(m)} F_{e,ij}^{(m)} \tag{2.96}$$

Total losses in gear mesh cycle for any control volume $H_{ij}^{(m)}$ which indicated by i, in all sequences of gear discretized movement $(m \in [0, M-1])$ for each gear in contact (subscript j) can be expressed in summation form as below:

$$P_p = \frac{1}{M}\sum_{m=1}^{M}\left[\sum_{j=1}^{J_1^{(m)}} P_{p,1j}^{(m)} + \sum_{j=1}^{J_2^{(m)}} P_{p,2j}^{(m)}\right] \tag{2.97}$$

The power losses due to oil pocketing for the *j*-th control volume at *m*-th rotational position of gear *i*, evaluated then an average of total losses is taken as main power loss.

2.7 Windage Power Losses

The concept of windage power losses refers to the air drag and air pocketing losses that have the same procedure as oil drag and pocketing losses with the difference that, air is a compressive fluid. Unlike oil, that density and volume assumed to be invariant, tremendous changes in air characteristics is not negligible. The eddy current around gear teeth and air compression between teeth affects the air pocketing action and is not straightforward to present as an exact model.

Generally, there are two different methods for modeling load independent losses; one is considering a mixture fluid of air and oil. In this method, there is no need of separating losses due to oil and air but an acceptable formulation must be developed for obtaining the equivalent fluid characteristics, density, viscosity and bulk module. Most of models that are dealing with blended fluid need revising coefficients from empirical tests to modify errors.

In models that wetted portion of gear separated from dry area, pure hydraulic and pneumatic analyses are done for each section. In this method, fluids are not affecting each other and penetration of air into oil is neglected. Losses due to pneumatic and hydraulic forces are calculated individually and by super positioning of effects, and by an empirical correcting coefficient, total losses are achieved.

In this study an equivalent viscosity and density is applied for windage power losses calculation that followed Anderson & Loewenthal model:

$$\boldsymbol{\rho}_{eq} = \frac{\boldsymbol{\rho}_{oil} + 34.25\boldsymbol{\rho}_{air}}{32.25} \tag{2.98}$$

$$\eta_{eq} = \frac{\eta_{oil} + 34.25\eta_{air}}{32.25}$$

By finding the lubricant characteristics, utilizing below equations for pinion and gear yeilds to total windage powerlosses [12]:

$$P_{W,g} = C_6\left(1 + 2.3\frac{b}{r_g}\right)\left(\frac{n_p}{m_g}\right)^{2.8} r_g^{4.6}\eta_{eq}^{0.2}\,(1 - (\frac{h_g}{2})) \tag{2.99}$$

$$P_{W,g} = C_6\left(1 + 2.3\frac{b}{r_g}\right) n_p^{2.8} r_p^{4.6}\eta_{eq}^{0.2}\,(1 - (\frac{h_p}{2}))$$

Where η_{eq} is equivalent dynamic viscosity and total windage power loss yeilds from summation of gear ($P_{W,g}$) and pinion ($P_{W,g}$) windage poower losses :

$$P_W = P_{W,g} + P_{W,p} \tag{2.100}$$

3 MODELING AND RESULTS

Applying MATLAB software for monitoring equations in chapter 2, helps to validate the accuracy of combination of different methods for modeling each losses. The platform of model is Anderson and Loewenthal's report [15] though it is done in 1980, it is still backbone of most of recent studies. Method of Xu [20] is applied for friction coefficient and substituted in base model for load dependent power losses.

Computing spin power losses contains bearing losses [27] and oil churning losses [25]. Load independent losses model is borrowed from one the most recent studies in Ohio State University. Validating the model is done by initializing the model by some known real life gearbox efficiency tests and finally comparing the results in each corresponding point. For instance the friction coefficient (μ) variation in the mesh cycle is plotted in Figure 3.1.

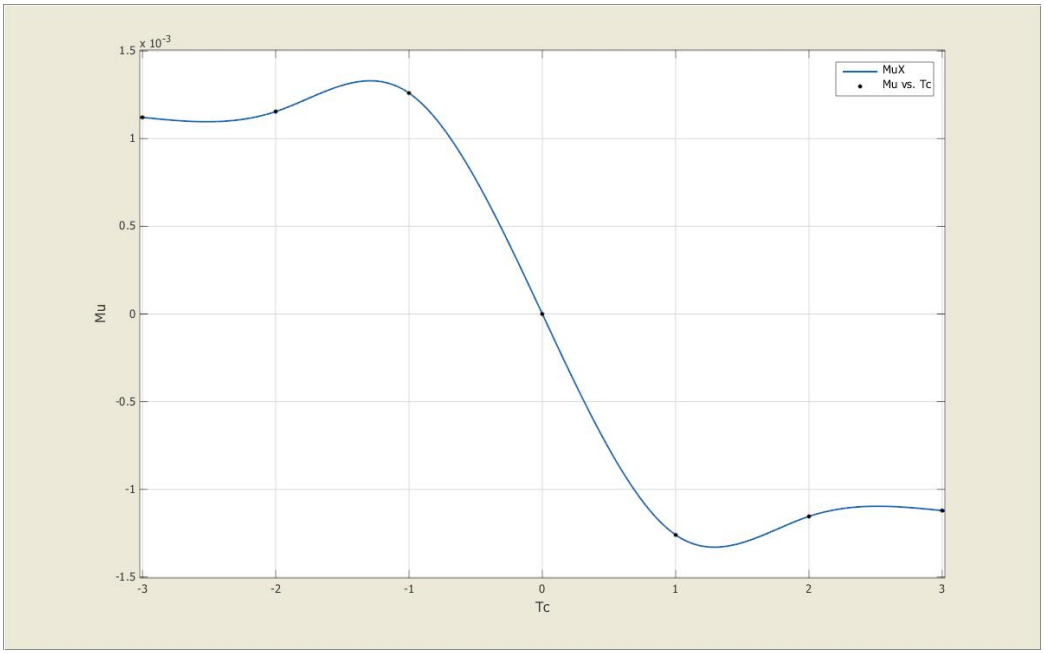

Figure 3.1. Friction cefficient variation in mesh cycle

As it was expected, friction coefficient (μ) vs. mesh cycle almost matches the corresponding graph in Xu's model. Differences due to geometry gradients is acceptable while lambda factor kept in between $4<\Lambda<10$.

3.1 Modeling of Step Gearbox

In modeling step gearboxes corresponding to each gear ratio, the characteristics of chosen gear should be taken into account for calculating the load dependent losses and according to the architecture of gearbox, spin losses should be considered for idling gears. For example in a 6-mode gearbox, the engaged gear pair causes load dependent losses and all of the rest gears, individually bring load independent power losses.

Since load dependent and spin losses are separated in the model, it is capable of handling any type of gear setup. Furthermore, all the possible losses have taken in to the calculations, so there is no compromising in any aspect and the model is almost complete according to the most recent discovered possible resistances in a gearbox.

The model is also capable of covering losses in a planetary gear set with an acceptable error. Whilst load dependent losses in sun-planet gear integration is the same when planet gears are stationary and for planet-ring gear mesh the situation is almost the same. However, for the situation where the output load is carried with planet carrier, relative speeds should be calculated considering planet orbiting as well. Load distribution on each gear and correspondingly gear teeth also is different for planetary gear set.

Spin losses in epicyclic is different comparing the system components. Since planet gears are in a bilateral contact with sun and ring gear, oil pocketing will be duplicated and oil drag resistance varies for two main reasons; firstly, the lubrication type is different and the orbiting planet gears and planet carrier have more oil drag resistance. Secondly, planet gear's plunge into oil bath and should be investigated because oil adhesion in surface is another power dissipation sink.

3.2 Single Reduction Gear

First it should be mentioned again that the method of calculation of friction coefficient has very important precaution that the lambda factor should be between 4 and 10 ($4<\Lambda<10$). Providing such condition needs to have very fine gear teeth surface and using high special synthesized oil for lubrication. These preconditions may demand more effort and budget but it is worthy to spend more budgets to have a transmission that is more efficient whilst there are lots of developments in DCTs and CVTs etc. to improve the performance and efficiency just little percentages. Furthermore, there is enough advancement in chemical ingredients of lubricants to have thin and robust lubricant film in between sliding and rolling parts.

***Table* 3-1** Gear pair geometries and operating parameters

Parameter	Symbol	Value
Gear pitch diameter, m	D_g	0.254
Pinion pitch diameter, m	D_p	0.1524
number of teeth of gear	N_g	80
number of teeth of Pinion	N_p	48
Diametral pitch , m	$D_{o,g}$	315
Pressure angle, deg	α_n	20
Helix angle	β	20
Tooth width	b	0.147
Lubricant dynamic viscosity, cP	η_m	50
Lubricant kinematic viscosity, cSt	ν_0	60
Lubricant friction factor	$\boldsymbol{f_L}$	7
Immersion level	H	0.5
Bearing thrust factor	Y_0	0.5
Bearing radial factor	X_0	0.6
Bearing bore diameter, m	D_b	0.07
Bearing friction factor	μ_b	0.002

Initializing the model by values been brought in below table led to an efficiency map for a single reduction gear transmission. Since there was no empirical equipment, the results were only evaluated by similar outcome of other studies. Furthermore, the new combination of equations and coefficients, which covers all of the power loss factors, makes the results in total power losses higher than what have been already investigated. It means that most of

studies on gear meshing power dissipation concentrated on a specific compartment of losses and used ready-made equations for the other losses without taking into consideration the effect of their assumptions and simplifications on the rest of equations.

Gear pair efficiency for variety of electric motor operation points with the ratio of 1.66:1 is calculated and values stocked in Table 3-2. The fact that gear ratios below 6:1 is more efficient and the reason of designing sequential gear boxes to reach higher ratios is evident where high rotational speed conveys low amount of torque. From below table, it can be seen that not only gear tooth deflection and different kind of wears increases in high gear ratio mates, power dissipation due to gear mesh losses will be more.

Since the main purpose of this study is to investigate the effect of power transmission on EVs' total energy consumption, efficiency map of gear pair that provided separately, should be combined with power electronics and electric machine efficiency map. Having a good understanding of efficiency of all components in powertrain makes it possible to design a proper arrangement of inverter, electric motor and transmission. Furthermore, in a situation that there are limitations in selecting one component, other compartments can design in a way that compensates drawbacks of restriction in choosing one specific part.

***Table* 3-2** Gear pair efficiency table

rpm / Torque	1000	2000	3000	4000	5000	6000	7000	8000	9000	10000
36	98,66	97,19	95,27	92,94	90,26	87,22	83,86	80,16	76,15	71,83
72	99,12	98,39	97,44	96,28	94,94	93,43	91,74	89,90	87,89	85,74
108	99,28	98,80	98,17	97,40	96,51	95,50	94,38	93,15	91,81	90,37
144	99,36	99,01	98,53	97,96	97,29	96,54	95,70	94,78	93,77	92,70
180	99,41	99,13	98,76	98,30	97,77	97,16	96,49	95,75	94,95	94,09
216	99,45	99,22	98,91	98,53	98,08	97,58	97,02	96,41	95,74	95,02
252	99,48	99,28	99,02	98,69	98,31	97,88	97,40	96,88	96,30	95,69
288	99,50	99,33	99,10	98,81	98,48	98,11	97,69	97,23	96,73	96,19
324	99,52	99,37	99,16	98,91	98,62	98,28	97,91	97,50	97,06	96,58
360	99,53	99,40	99,21	98,99	98,72	98,42	98,09	97,72	97,32	96,89

By using output data of gearbox model, sweet spots of electric drive may not remain the best operating points according to corresponding efficiency of gearbox. Regarding to

Figure 3.3 although the efficiency does not vary a lot in accordance to sweet spots in Figure 3.4 but these small variations when are multiplied to each other yield to a considerable power consumption over a driving cycle. Increasing powertrain efficiency has peripheral advantages that have positive effects on not only total vehicle efficiency but also the vehicle performance.

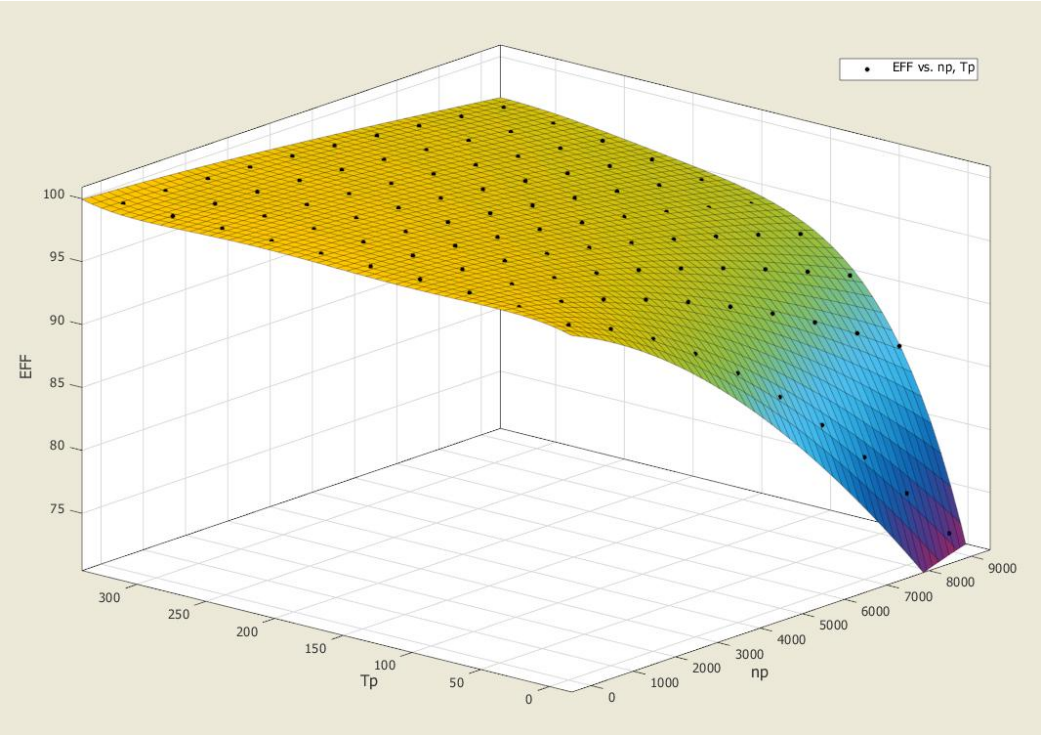

Figure 3.2. Gear pair 3D efficiency map

The amount of consumed energy multiplied by even small fraction of percentage finally brings a considerable power loss. It will be more determinant when variable gear ratio selections are available.

After validating the model, it will embedded into a complete vehicle simulation and total efficiency in corporation of corresponding working point efficiency of gearbox and other components will obtain. In an overlapped map, it can be recognized why electric vehicle power drops significantly at high speeds. Although electrical components are working in a semi constant power in a wide range of speed and torque variety, but gear box efficiency decreases radically in high speed and low conveying torque.

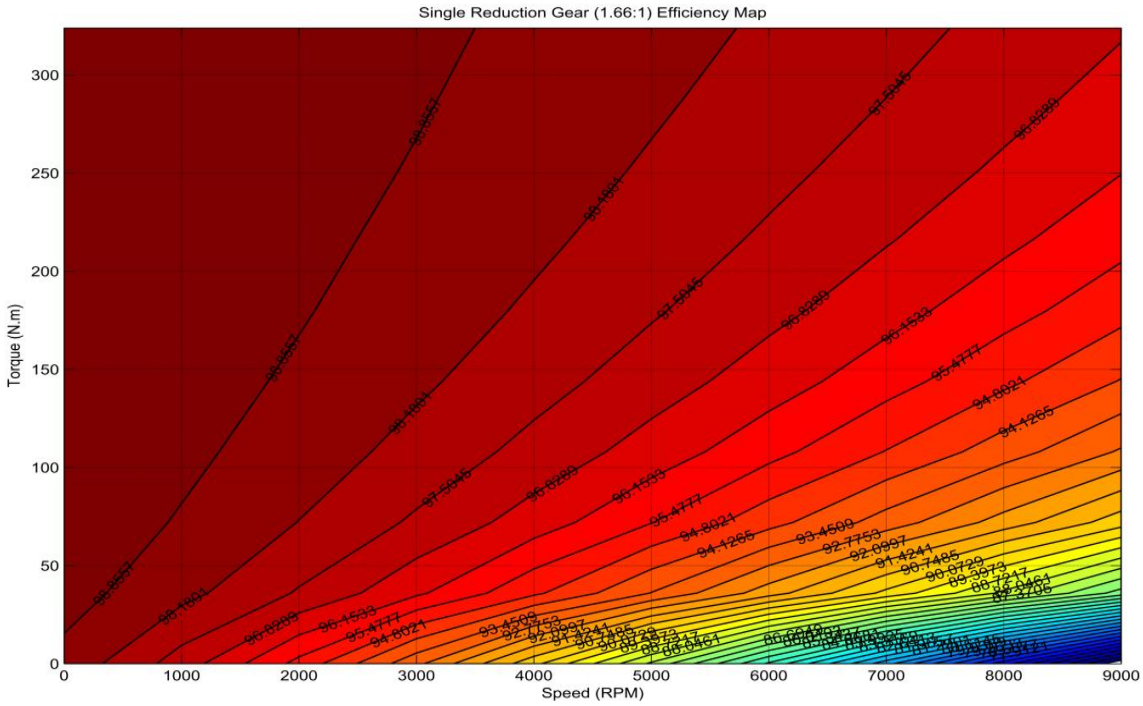

Figure 3.3. Gear pair 2D efficiency map

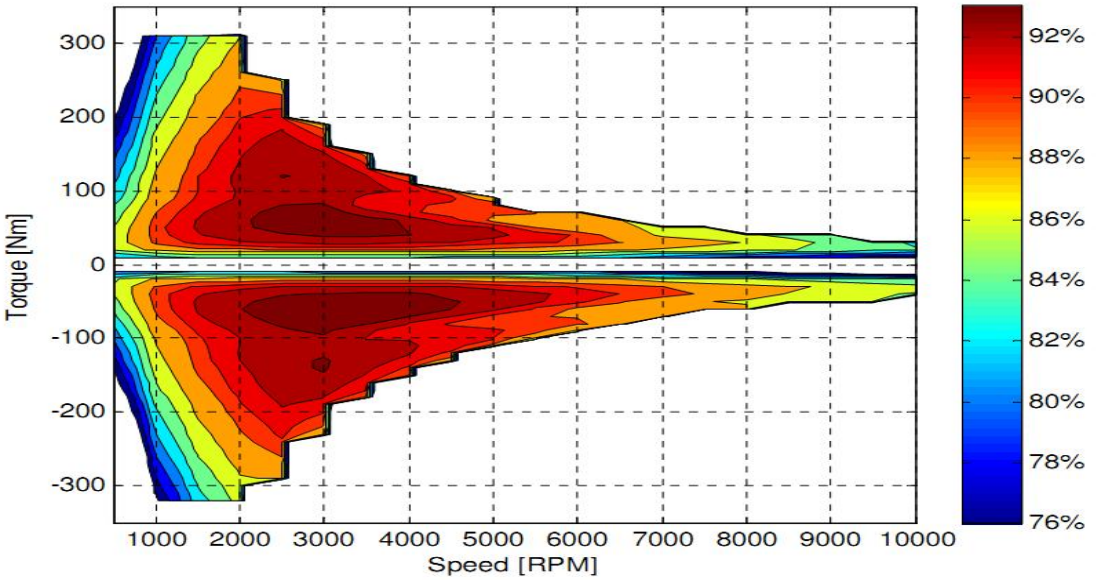

Figure 3.4. Electric motor efficiency map

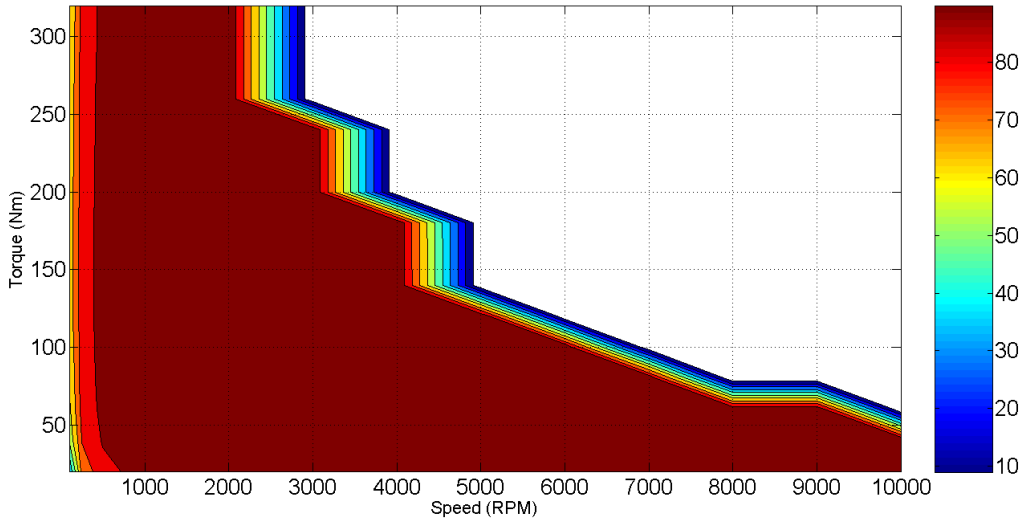

Figure 3.5. Power Electronic Efficiency Map

As mentioned above a combination of electronic and mechanical efficiency should develop for overall efficiency of powertrain in EVs. By assuming a constant efficiency of 96.85% for inverter, final efficiency in most centered spot still varies by gearbox efficiency from 98.18% to 95.47%. By assuming that electric motor is kept in its most efficient contour of operation by 93%, the final efficiency of powertrain from batteries to wheels will be:

$$\eta_{batt-wheel} = \eta_{inverter}\,\eta_{motor}\,\eta_{GB} \tag{3.1}$$

$$\eta_{batt-wheel} = 96.85\% \times 93\% \times (98.18\%\sim 95.47\%) = 88.43\%\sim 85.99\%$$

Now if the two separate operating point of electric motor with the same power but different corresponding torque and rotational speed and also different electric and mechanical efficiency takes into comparison, the point with lower electric efficiency (η_{motor}=91%) but higher gearbox efficiency (η_{GB}=98.85%) has a higher total efficiency of 87.12% than the other point by higher electric efficiency (η_{motor}=93%) but lower gearbox efficiency (η_{GB}=95.47%) which is 85.99% .

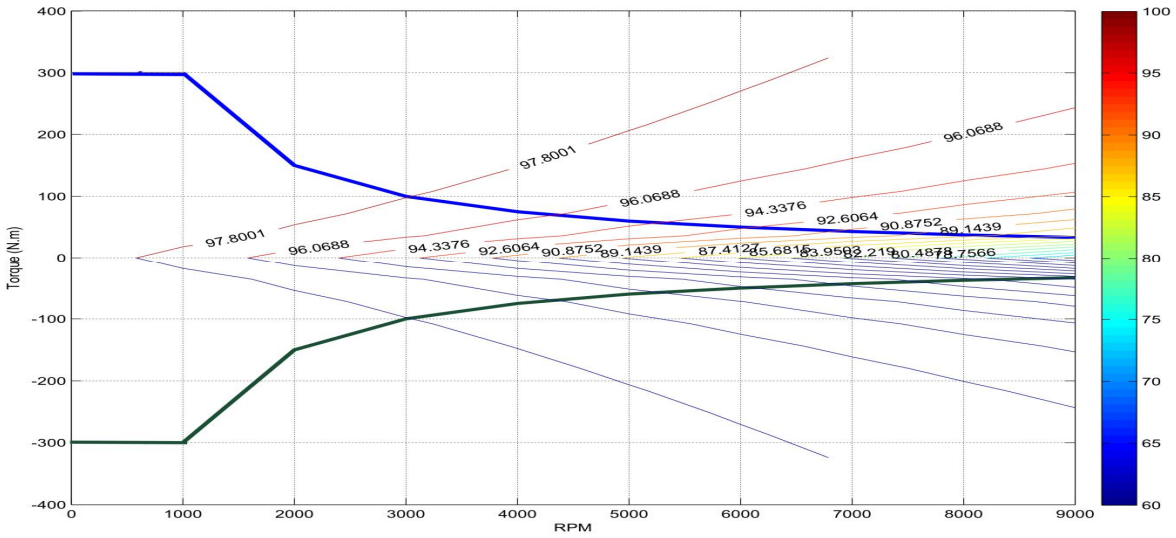

Figure 3.6. typical electric motor operation including gearbox efficiency curves

3.3 Multi Step Gearbox

In conventional variable stepped transmission with counter shaft, there is a pair of gears for each step. Assuming diametral pitch equals to 315, the ratio of 1.66:1 for countershaft and 3.5:1 for differential, typical ratios for each gear will be:

***Table* 3-3** Gearbox ratios

Shifting stage	Ratio	Pinion diameter	Gear diameter	Final ratio
1st	2.02:1	0.04	0.0808	11.76:1
2nd	1.5:1	0.05	0.075	7.175:1
3rd	0.79:1	0.065	0.05135	4.62:1
4th	0.58:1	0.085	0.0493	3.39:1
5th	0.46:1	0.09	0.0414	2.66:1

Neglecting dog clutches and synchronizers losses, for each stage load dependent and spin losses are calculated for selected gear pair. For the rest of gear pairs only spin losses take in to consideration. Appling the model on NEDC and finding portion of each gear configuration yields to find the total losses during the driving cycle. For this mean, operation of a typical electric motor can be used and assuming that it operates between

2000 rpm and 5000 rpm and wheels diameter of 0.7 m the motor rotational speed to vehicle speed calculates as below in km/h:

$$V_{vehicle} = 0.1886(\Omega_{motor}\ r_{final}\ D_{wheel}) \quad (3.2)$$

Neglecting resistive forces and dynamic inertia of vehicle, shifting steps from zero to 248 km/h is illustrated in Figure 3.8. So by initializing demanded power of electric motor, portion of each gear can be obtained through the figure. The strategy of selecting proper gear ratio is not under scope of this study, but can be investigated after running driving cycle with different power consumption.

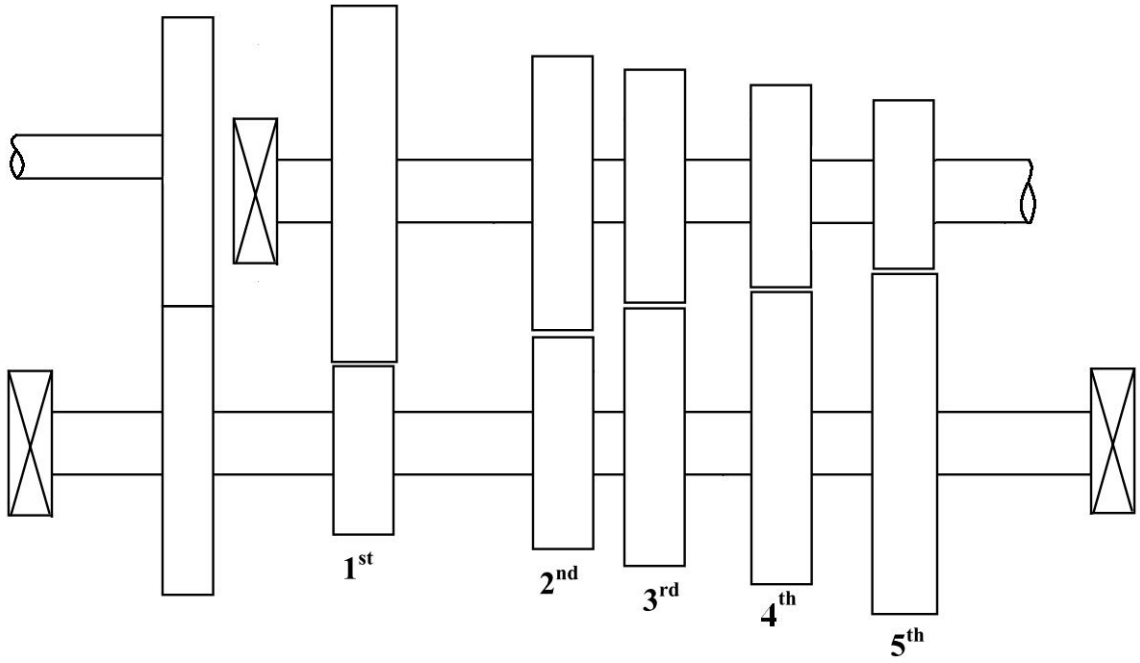

Figure 3.7. Schematic 5 Stage Gearbox

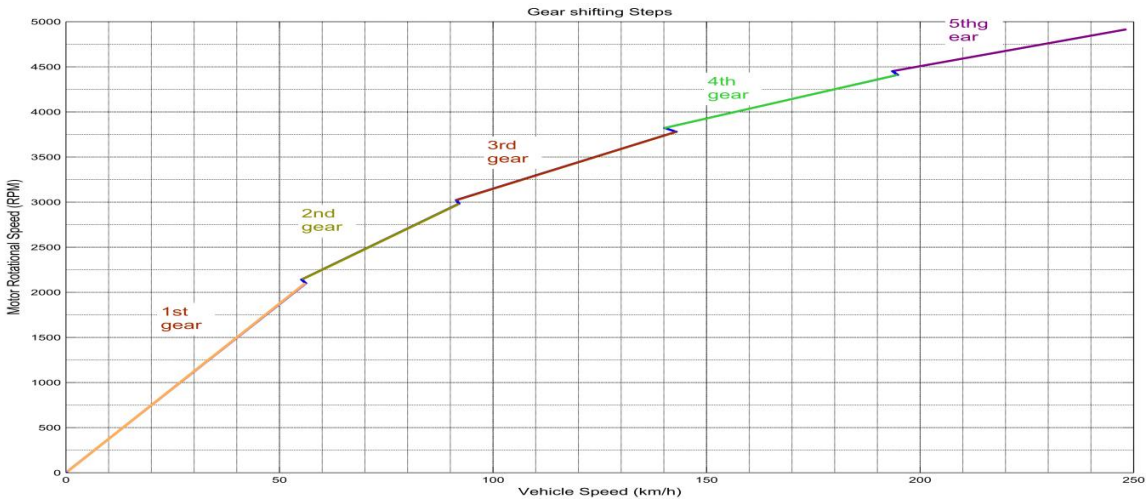

Figure 3.8. Gear Shifting Steps

Modifying the model for a multistep transmission just needs to diagnose the load conveying gear pair from the rest of idling gear pairs and applying below equation:

$$P_{load} = \sum_{N_l} (P_{si} + P_{ri} + P_{b,Li}) \tag{3.3}$$

$$P_{spin} = \sum_{N_i} (P_{di} + P_{fi} + P_{pi} + P_{Wi} + P_{b,Vi})$$

$$P_{LOSS} = P_{load} + P_{spin}$$

Load distribution on each gear and supporting bearings calculates by the arrangement of gearbox for any case.

4 SIMULATION AND RESULTS ANALYSIS

As discussed in chapter one, in order to monitoring EVs' performance in various operations, different driving cycles have defined. The driving cycle which is taken into simulation in this study is NEDC which is shown in Figure 4.1. Whereas the effect of gearbox efficiency is the concern of simulation, all the parameters for vehicle characteristics are virtual and tried to be wise values close to a real typical sedan car.

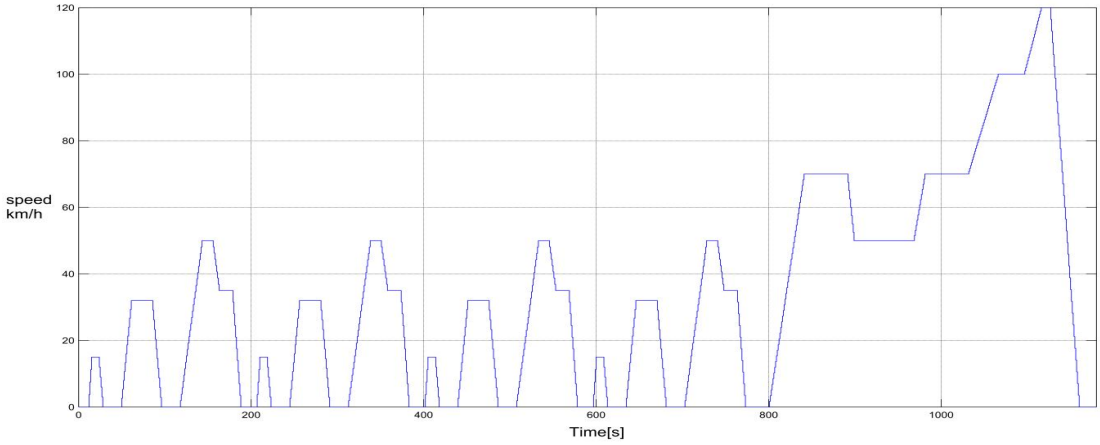

Figure 4.1. New Eurpean Driving Cycle

Environmental physical parameters like gravitational acceleration and air density are also chosen roughly in Table 4-1.

***Table* 4-1** Vehicle Parameters

Air density in kg/m^3	1.225
Gravitational acceleration in m/s^2	9.81
Mass of the vehicle in kilograms	1600
Vehicle frontal area in square meters	2.25
Air drag coefficient	0.40
Tire rolling resistance coefficient	0.015
Dynamic rolling radius of the tire in meters	0.296
The moment of inertia of the bodies "before" the reduction gear: motor rotor, gear input shaft in kg. m^2	0.2
The moment of inertia of non-driving axle and bodies "after" the reduction gear: output shaft, differential, drive shafts, wheels, brakes... in kg. m^2	2
Efficiency of regenerative braking	0.4

Taking estimated values for building vehicle simulation (Figure 1.1) by utilizing MATLAB SIMULINK led to calculation of energy consumption for producing power that can carries the vehicle according to driving cycle demands. Different type of transmissions and gear ratios are applied for same vehicle and driving cycle in following compartments.

4.1 Integrating a Single Reduction Model in the Simulation

In the most of currently used EVs, variable transmission excluded from the powertrain so that whole vehicle demanded performance covered by electric motor rotational speed domain. Changing the gear ratio does not affect EVs' power performance whilst according to PMSM (the most common electric motor type in EVs and HEVs powertrain) principle; output power is constant after passive rotational speed whereas output torque is fixed.

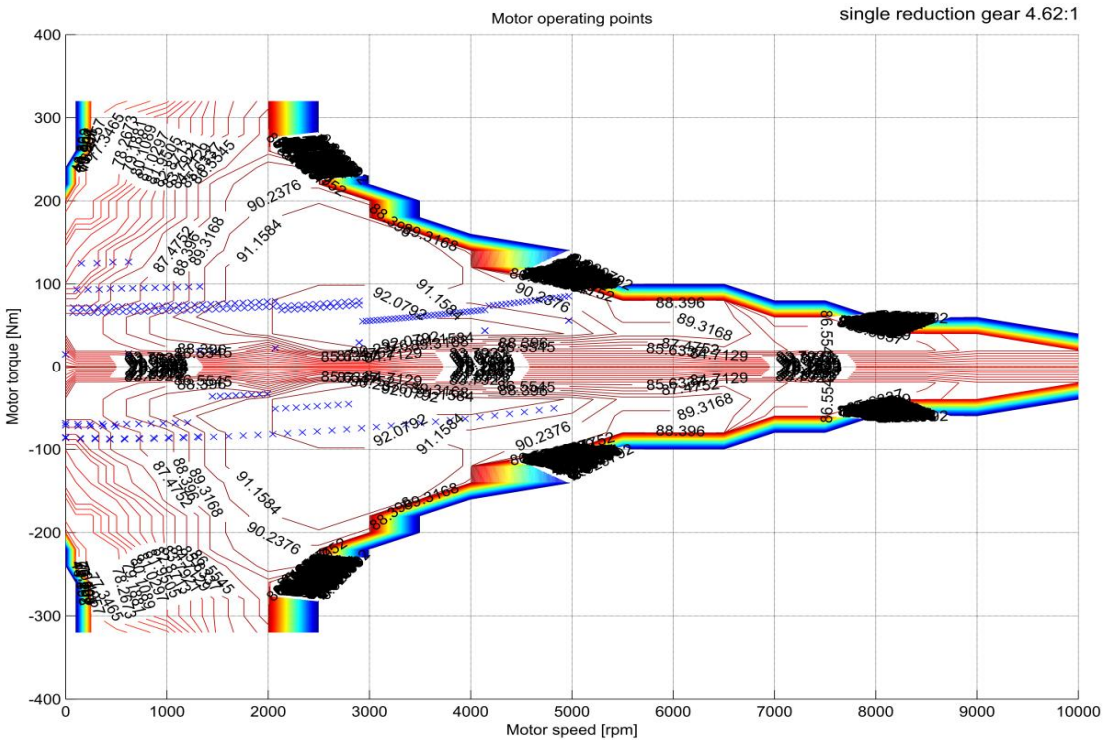

Figure 4.2. Motor Operation With Single Reduction Gear

First simulation is run with a single reduction ratio of 4.62:1. Power consumption, maximum demanded torque and power were:

Max power (kW) = 44.352

Energy/km (kWh) = 0.1651

Max torque(Nm) = 126.4163

In Figure 4.2, electric motor operating points plotted on electric motor efficiency map and it can be seen that maximum speed of 120 km/h reached on 5000rpm. Considering the gear efficiency (Figure 4.4) and driving cycle (Figure 4.1), it is visible that the reduction gear efficiency drops in high speeds. For a city car, best option would be a single gear that is simpler, more compact and lighter which are the most determinant factors affect the vehicle design.

The gear mesh efficiency map, is not included in Figure 4.2, so the most efficient operating of whole powertrain is not the same as sweet spots of electric motor. It means that separate points in motor efficiency map with different efficiency may lead to the same total efficiency when multiplied with other compartment efficiency in powertrain. However, the ratio of reduction gear is dependent on vehicle maximum demanded speed and propulsion motor rotational speed limit. Therefore, the only variable parameter for improving the powertrain efficiency refers to electric motor design.

When vehicle moves at higher speeds, resistive forces are increasing. Air drag force develops by second power of car linear speed and higher angular speed of tires leads to bigger dynamic wheel radius. Rolling fiction coefficient is also related to square root of contact point velocity. Therefore, the higher vehicle linear speed yields to higher resistive force.

While the electric motor has to run faster to pivot wheels to reach high speed, it also has to provide higher torque to overcome resistive forces such as rolling friction and air drag which have increased by growth of vehicle speed. So, both load dependent and spin power losses in gearbox will increase. Electric motor and power electronics efficiency (regarding to Figure 3.4 and Figure 3.5) are not in the most efficient point in corresponding power point. Taking into account all of above factors, radical incline of power consumption in Figure 4.3 can be explained.

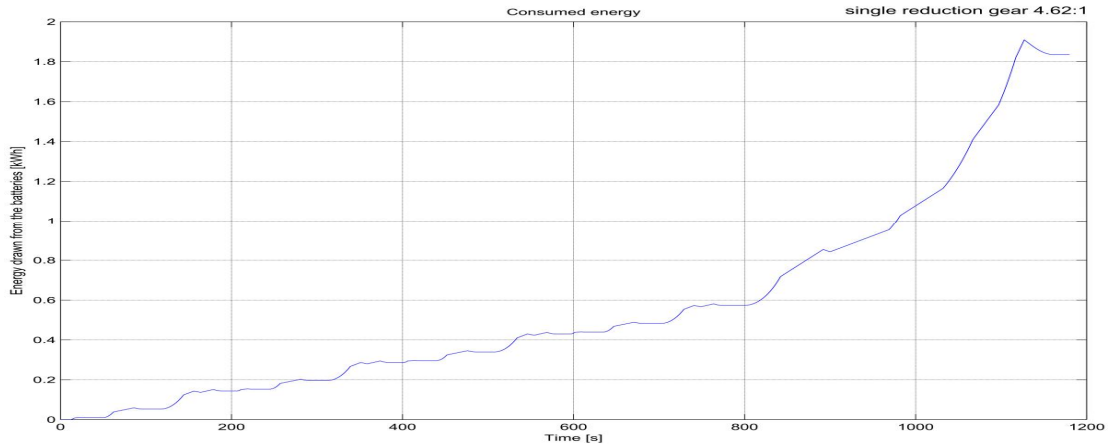

Figure 4.3. Total energy consumption

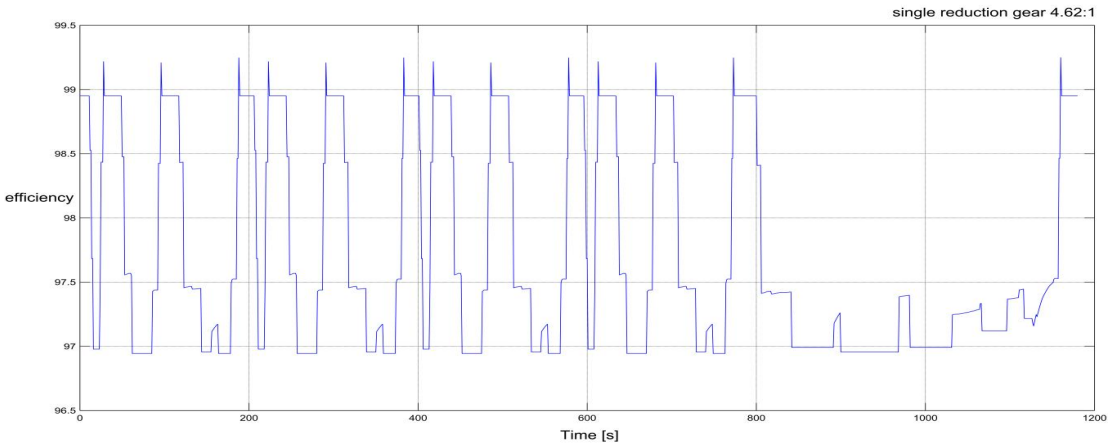

Figure 4.4. Gear Mesh Efficiency

4.2 Embedding Multi Step Model in the Simulation

As discussed in chapter 4.1, the increment of power extraction from batteries can be divided into two main categories; environmental (road condition) and powertrain power dissipation. Finding a solution for an advantageous powertrain design (that is the aim of this study), needs compromises between all of powertrain compartments efficiency. For instance, the same power can be obtained from electric motor in speed of 120 km/h in more efficient operation point just by reducing the rotational speed and increasing the torque. This can be possible only with a variable transmission.

Substituting a variable transmission to the powertrain imposes extra weight, more space occupation, higher production cost etc. to vehicle general design that brings more limitations and complications. Despite of its drawbacks on other designing factors, in powertrain itself, more rotating parts means more power dissipation.

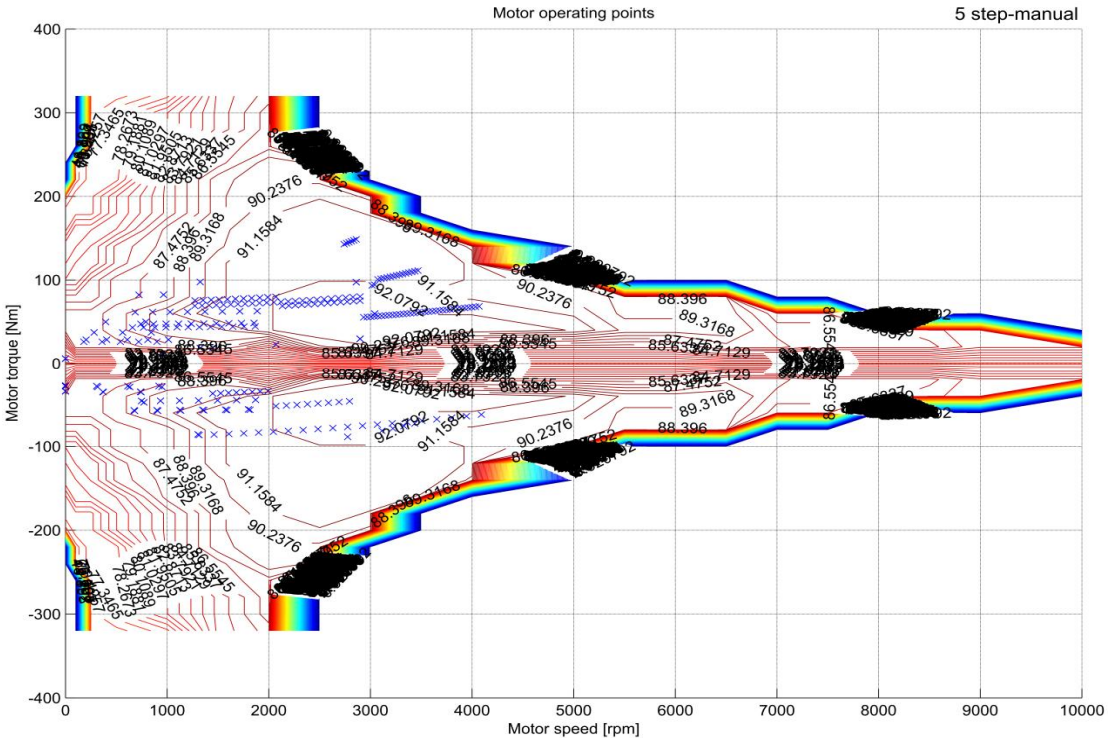

Figure 4.5. Motor Operation With 5step Gearbox

Firstly, an ideal variable gearbox with the efficiency of single gear is embed to the vehicle simulation and as it was expectable; the vehicle total energy consumption per kilometers was 2 Wh lower than a single reduction gear that means 1.2% more efficiency. It can be seen from comparison between Figure 4.2 and Figure 4.5 that motor operating points with 5-step transmission are in better efficiency contours.

Nevertheless, the energy consumption and gearbox efficiency trend (Figure 4.6 and Figure 4.7) is so close to the single reduction mode, by considering a real gearbox, losses due to gearbox components yield to 1.7 Wh more energy consumption/km, which is 1% less efficient. Output data of simulation is brought below:

Max power (kW) = 44.51

Energy/km (kWh) = 0.1668

Max torque(Nm) =148.58

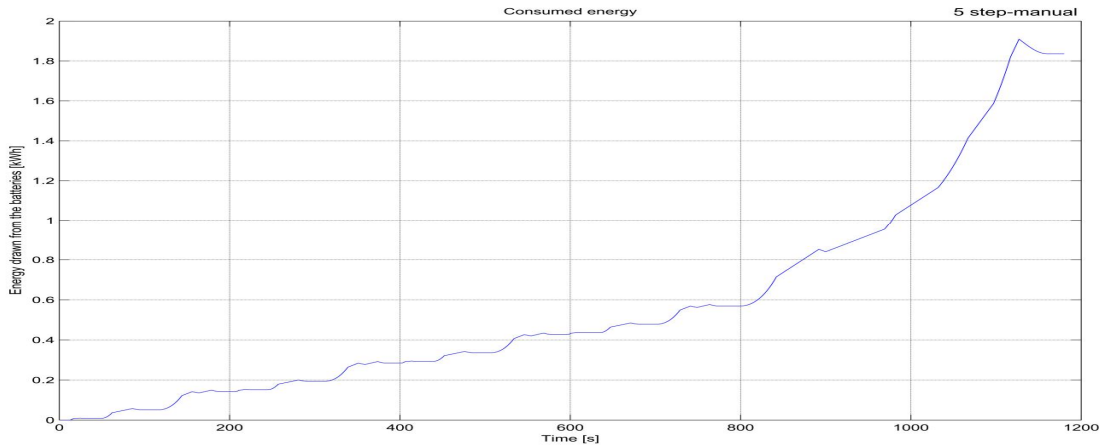

Figure 4.6. Total Energy Consumption

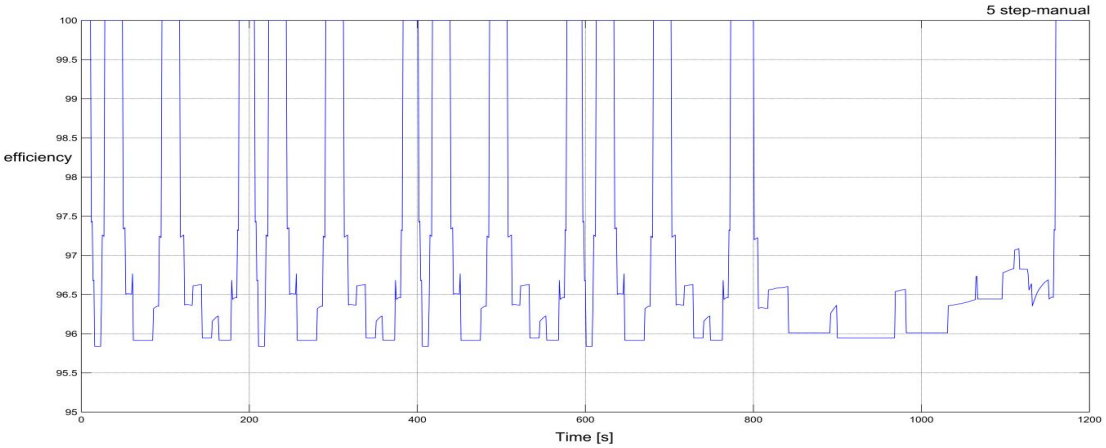

Figure 4.7. Five Step Gearbox Efficiency

According to the gears ratio in 5-step gearbox and gear shifting strategy that is optimized, not only the energy consumption is not improved but the maximum needed torque and power is increased. One of the reasons for incline in maximum torque and power can be the more rotating mass in gearbox that has bigger moment of inertia. It makes the designing procedure more restricted because the chosen electric motor should be stronger.

4.3 Embedding CVT Model in the Simulation

Defining the gear ratio selection strategy as a continuously variable transmission that keeps the electric motor operation as close as possible to its most efficient point without any restriction in ratio is done in third simulation. However, the type CVT and its efficiency is unknown, the simulation ran for a virtual CVT with the same efficiency as single reduction gear. The effect of utilizing infinite ratio can be seen Figure 4.8 where electric motor operating points are concentrated on the sweetest spot.

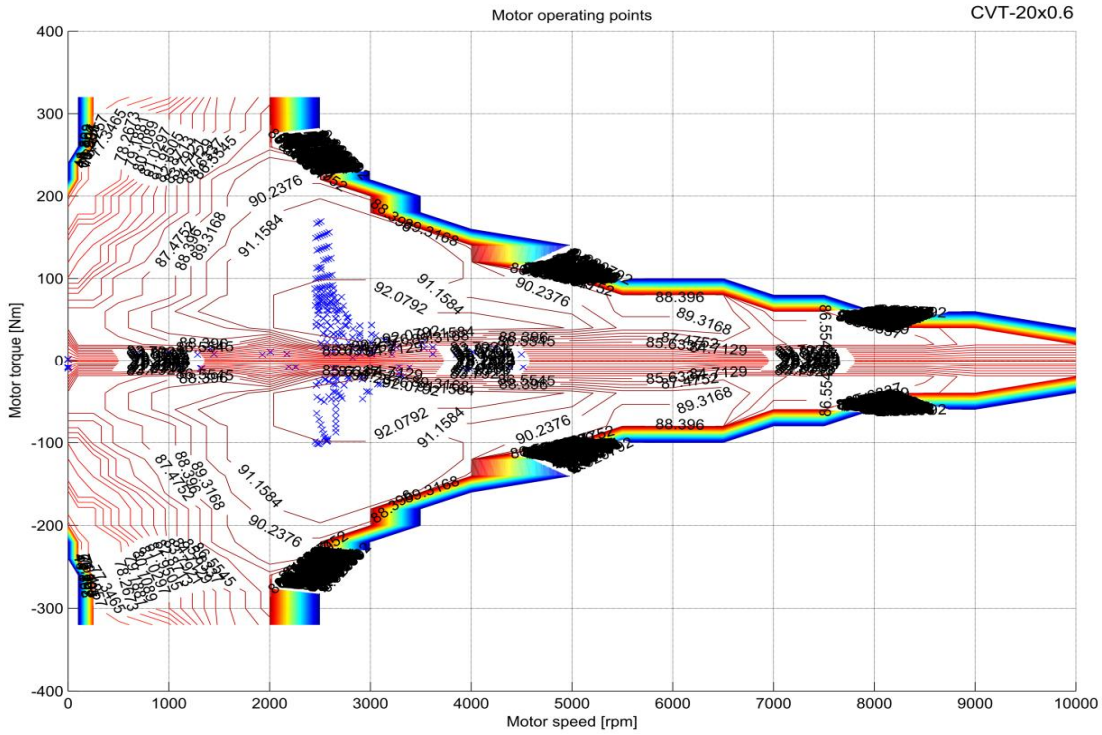

Figure 4.8. Motor Operation With a CVT

The energy consumption in this mode is the lowest. Comparing to single reduction gear with fixed ratio, with CVT energy consumption is 3.5 Wh lesser and correspondingly it is 2.1% more efficient.

Max power (kW) = 43.86

Energy/km (kWh) = 0.1616

Max torque(Nm) = 166.9547

The maximum needed power is about 0.5 kW less than single gear but the maximum demanded torque is about 40.5 Nm more and it is the side effect of very low ratio in vehicle's high speeds that should compensate the smaller motor angular speed in order to provide enough power on the wheel. Extracted energy form batteries stays in the same shape (Figure 4.9) but at lower value in all corresponding points.

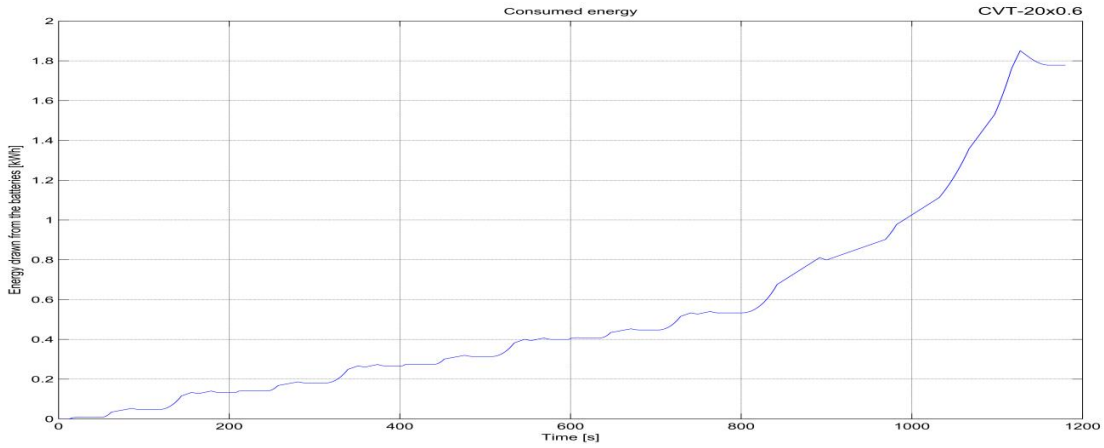

Figure 4.9. Energy Consumption CVT

In (Figure 4.10) where green circles are representing motor operating point and blue crosses the single reduction gear, it can be understood that what a CVT does is to shift demanded power points along constant power curves to more efficient area of electric motor operation. As assumed that CVT has the same efficiency as single reduction gear, regarding to (Figure 4.11), power train efficiency is not only better considering the electric motor efficiency but the operating points stay in higher level of transmission efficiency.

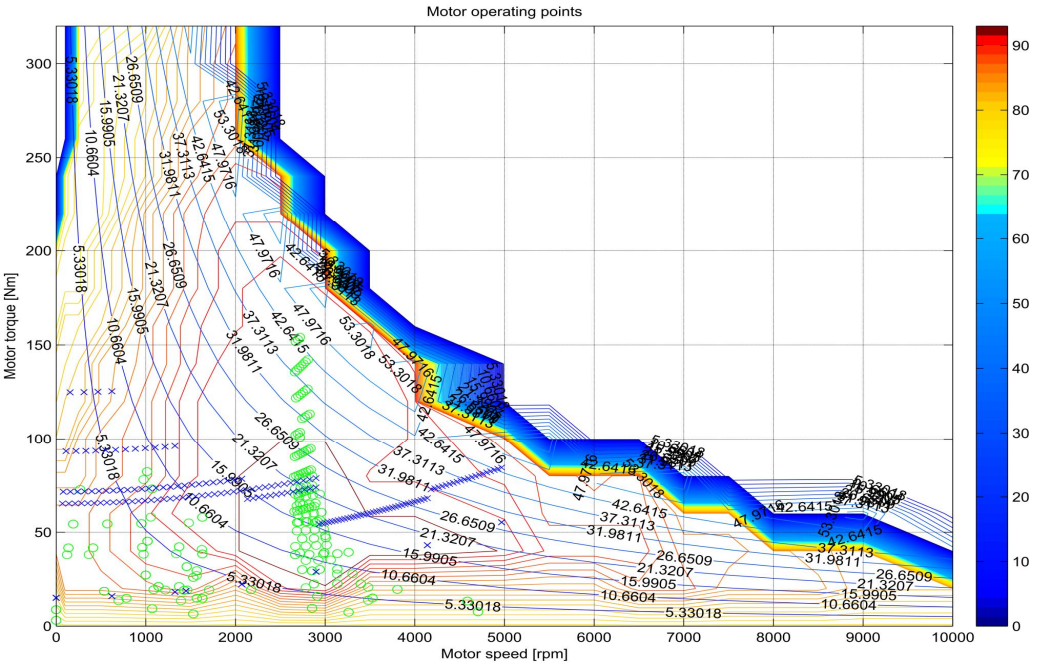

Figure 4.10. Motor operating points CVT vs. Single Gear

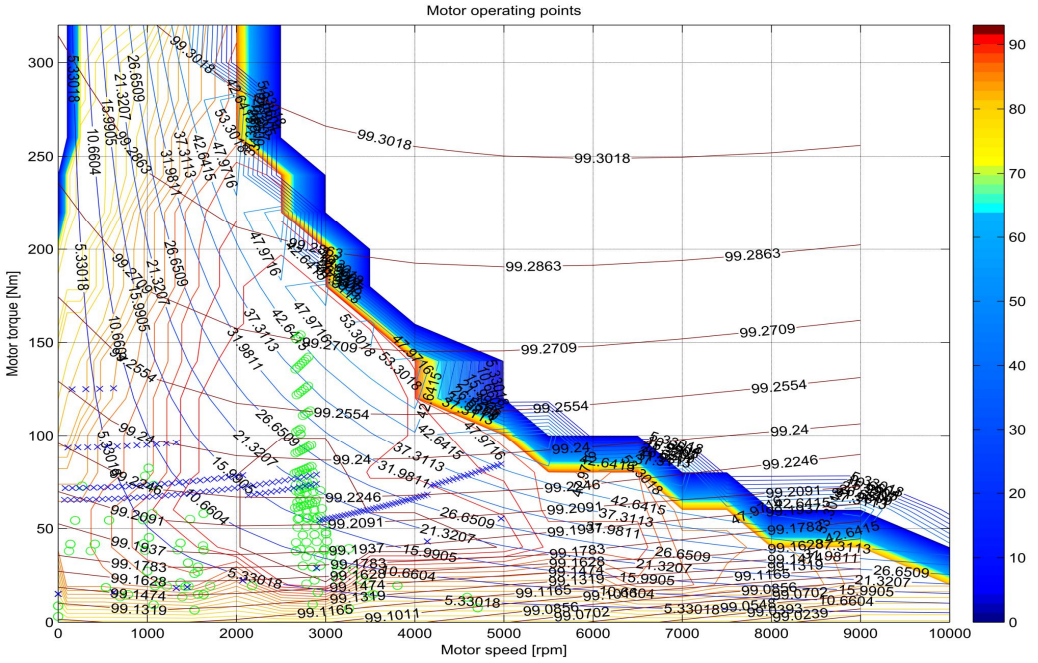

Figure 4.11. Motor operating points CVT vs. Single Gear efficiency plus curves

5 CONCLUSIONS

In this study, a combination of the most recent methods applied and to develop a general-propose model for mechanical efficiency of gear pairs. Power losses in gear mesh divided into two main sub losses: load dependent and spin losses. Classic physics rules in fluid dynamics and thermodynamics are utilized for modeling of lubricant effect on gears movement. Then the model is employed for prediction of power loss in parallel axis gear mesh in conventional gearboxes. Validation of model is done by comparison of results with the same initial values of previous studies.

All of the components of power transmission in an EV have been investigated and including of gearbox model, a simulation model for electric vehicle energy consumption was developed. Three main type of transmission embedded in the simulation and results compared regarding to total vehicle energy consumption. According to the provided model for gear mesh, gear ratio selection strategy and efficiency maps of power electronics and electric motor, the most efficient option for transmission is a CVT with the same power losses as a single reduction gear. The second proper option is a single reduction gear and a 5-step gearbox would be the last.

In this study, only efficiency of parallel helical gear mesh is investigated, but the provided model can be modified for epicyclic gears as well. Furthermore, for all of simulation models, the ratio selection strategy is built in a way that the total combined efficiency of both electrical and mechanical components stays in the highest possible state. Another recommendation for future work would be the optimization of gear ratios and strategy of gear selection.

6 REFERENCES

[1] N.Kheira, M.S. Salmanb, and N.J.Schoutenaa; Electrical and Systems Engineering Department, School of Engineering and Computer Sciences, Oakland University, 102A SEB, Rochester, MI 48309, USA.General Motors Research and Development Center, 30500 Mound Road, Warren, MI 48090, USA Available online 7 January 2004.

[2] J. Amirault, J.Chien, S.Garg, D.Gibbons, B.Ross, M.Tang, J.Xing, I.Sidhu, P.Kaminsky, and B.Tenderich; 2009.9.v.1.1, Revision Date: December 21, 2009.

[3] Stephen J. Chapman; ELECTRIC MACHINERY FUNDAMENTALS FOURTH EDITION,2004, ISBN 0-07- 246523-9.

[4] J.Puranen ; Induction motor versus permanent magnet synchronous motor in motion control applications: a comparative study Lappeenranta 2006; ISBN 952-214-296-4.

[5] T.L.Krantz and R.F.Handschuh; Propulsion Directorate; U.S. Army Aviation Research and Technology Activity-AVSCOM; Lewis Research Center; Cleveland, Ohio 1990 NASA AVSCOM; Technical Memorandum 90-C-005.

[6] F.L.Litvin; A.Fuentes, D.Vecchiato; I. Gonzalez-Perez; New Design and Improvement of Planetary Gear Trains; University of Illinois at Chicago, Chicago, Illinois & U.S Army Research Laboratory NASA/CR—2004-213101- ARL–CR–0540.

[7] JJ Coy, DP Townsend, EV Zaretsky, "Gearing", NASA Reference Publication 1152, AVSCOM Technical Report 84-C-15, 1985.

[9] S.He, S.Cho, R.Singh; Prediction of dynamic friction forces in spur gears using alternate sliding friction formulations; Journal of Sound and Vibration 309 (2008) 843–851.

[10] Song He; EFFECT OF SLIDING FRICTION ON SPUR AND HELICAL GEAR DYNAMICS AND VIBRO-ACOUSTICS; The Ohio State University 2008.

[11] J.Packer; Improved method for the calculation of friction losses in spur and helical gears; Ricardo UK Ltd 2006.

[12] N.E.Anderson and S.H.Loewenthal; Comparison of Spur Gear Efficiency; Propulsion Laboratory, U.S. Army Research and Technology Laboratories (AVRADCOM), NASA Lewis Research Cente 1981Prediction Methods.

[13] M.Vaishya, R.Singh; Department of Mechanical Engineering, The Ohio State University,Columbus,OH 43210-1107; Transactions of the ASME; Vol. 125/388 , JUNE 2003.

[14] J.A.de Marchi; MODELING OF DYNAMIC FRICTION, IMPACT BACKLASH AND ELASTIC COMPLIANCE NONLINEARITIES IN MACHINE TOOLS,WITH APPLICATIONS TO ASYMMETRIC VISCOUS AND KINETIC FRICTION IDENTIFICATION; Rensselaer Polytechnic Institute,Troy, New York;December 1998.

[15] N.E.Anderson and S.H.Loewenthal; Spur-Gear-System Efficiency at Part and Full Load; NASA Scientific and Technical Information Office 1980.

[16] P. A. Simionescu (1998-09-01). "A Unified Approach to the Assembly Condition of Epicyclic Gears". ASME Journal of Mechanical Design 120 (3): 448–453.

[17] S.He, S.Cho, R.Singh; Prediction of dynamic friction forces in spur gears using alternate sliding friction formulations; Journal of Sound and Vibration 309 (2008) 843–851.

[18] Y. Michlin, V. Myunster; Determination of Power Losses in Gear Transmissions with Rolling and Sliding Friction Incorporated; mechanism and Machine Theory 37 (2002) 167.

[19] H. Xu, A. Kahraman, N. E. Anderson, D. G. Maddock; Prediction of Mechanical Efficiency of Parallel-Axis Gear Pairs; ASME Journal 58 / Vol. 129, JANUARY 2007.

[20] H.Xu; DEVELOPMENT OF A GENERALIZED MECHANICAL EFFICIENCY PREDICTION METHODOLOGY FOR GEAR PAIRS; The Ohio State University 2005.

[22] K. L. Johnson and K. Kendall and A. D. Roberts, Surface energy and the contact of elastic solids, Proc. R. Soc. London A 324 (1971) 301-313.

[21] S. Baglioni, F. Cianetti, L. Landi; In fl uence of the addendum modi fi cation on spur gear ef fi ciency; Università degli Studi di Perugia, Dipartimento di Ingegneria Industriale, via G. Duranti 63, 06125 Perugia, Italy 2010.

[22] K. L. Johnson and K. Kendall and A. D. Roberts, Surface energy and the contact of elastic solids, Proc. R. Soc. London A 324 (1971) 301-313.

[23] Hamrock, B. J.; and Dowson, D.: Isothermal Elastohydrodynamic Lubrication of Point Contacts. III - Fully Flooded Results. J. Lub. Tech., vol. 99, no. 2, Apr. 1977, pp. 264-276.

[24] M. Kolivand , S. Li, A. Kahraman; Prediction of mechanical gear mesh efficiency of hypoid gear pairs; Gear and Power Transmission Research Laboratory, The Ohio State University, 201 W. 19th Avenue, Columbus, OH 43210, USA; 2010.

[25] S.Seetharaman; AN INVESTIGATION OF LOAD-INDEPENDENT POWER LOSSES OF GEAR SYSTEMS; The Ohio State University; 2009.

[26] Streeter, L. V., and Wylie, E. B., 1985, Fluid Mechanics, Eighth edition, McGraw-Hill, New York.

[27] Khonsari, M. M., Booser E. R., “Applied Tribology, Bearing design and Lubrication”, John Wiley & Sons, 2001.

[28] Pechersky, M. J. and Wittbrodt, M. J., 1989, “An analysis of fluid flow between meshing spur gear teeth,” Proceedings of the ASME 5th International Power Transmission and Gearing Conference, Chicago, 335–342.

[29] Engineering-abc.com. Equivalent bearing load. [Online] Available from: http://www.tribology-abc.com/calculators/pe.htm. Retrieved 13.11.2012.

Appendix

Appendix A

***Table* 6-1** Constants used in gear loss equations

Constants	Value for SI unit	Value for U.S. customary unit
C_1	29.66	45.94
C_2	9.0×10^{7}	1.3×10^{4}
C_3	1×10^{-3}	1.515×10^{-4}
C_4	2.04×10^{-8}	2.70×10^{-13}
C_5	0.019	2.86×10^{-9}
C_6	2.82×10^{-7}	4.05×10^{-13}
C_7	6894	2051
C_8	6894	1.0
C_9	1.05×10^{-4}	1.59×10^{-5}
C_{10}	0.0254	1.0
C_{11}	2.051×10^{-7}	4.34×10^{-3}
C_{12}	1×10^{-3}	4.629
C_{13}	6.8×10^{-5}	0.303
C_{14}	1.0	1.5×10^{-6}

Appendix B

***Table* 6-2** Equations for path of contact

Parameter	Symbol	Formula
Length between interference points, m	X_A	$(\boldsymbol{D_p + D_g})^{\mathbf{1/2}}$
Start of double-tooth contact, m	X_1	$X_A - 0.5(D_{a,g}^2 - D_{o,g}^2)^{1/2}$
End of single-tooth contact, m	X_3	$X_1 + \mathcal{P}_o$
End of mesh cycle, m	X_4	$0.5(D_{a,g}^2 - D_{o,g}^2)^{1/2}$
End of double-tooth contact, m	X_2	$X_4 + \mathcal{P}_o$
Pitch point, m	$X_{\mathcal{P}}$	$X_1 + C_{10}\sqrt{\left(\frac{2 + N_p m_g}{2p}\right)^2 - \left(\frac{N_p m_g \cos\beta}{2p}\right)^2} - C_{10}\frac{N_p m_g \sin\beta}{2p}$
Midpoint between Xl and X2, m	ℓ_1	$(X_1 + X_2)/2$
Midpoint between X3 and X4, m	ℓ_2	$\ell_1 - X_1 + X_3$
Length of single-tooth contact, m	ℓ_3	$X_4 - X_3 + X_2 - X_1$
Start of double-tooth contact, m	ℓ_4	$X_2 + 3 \times 10^{-5}$
Length of double-tooth contact, m	ℓ_5	$X_3 - X_2$
Total length of contact, m	ℓ_6	$X_4 - X_1$

Appendix C

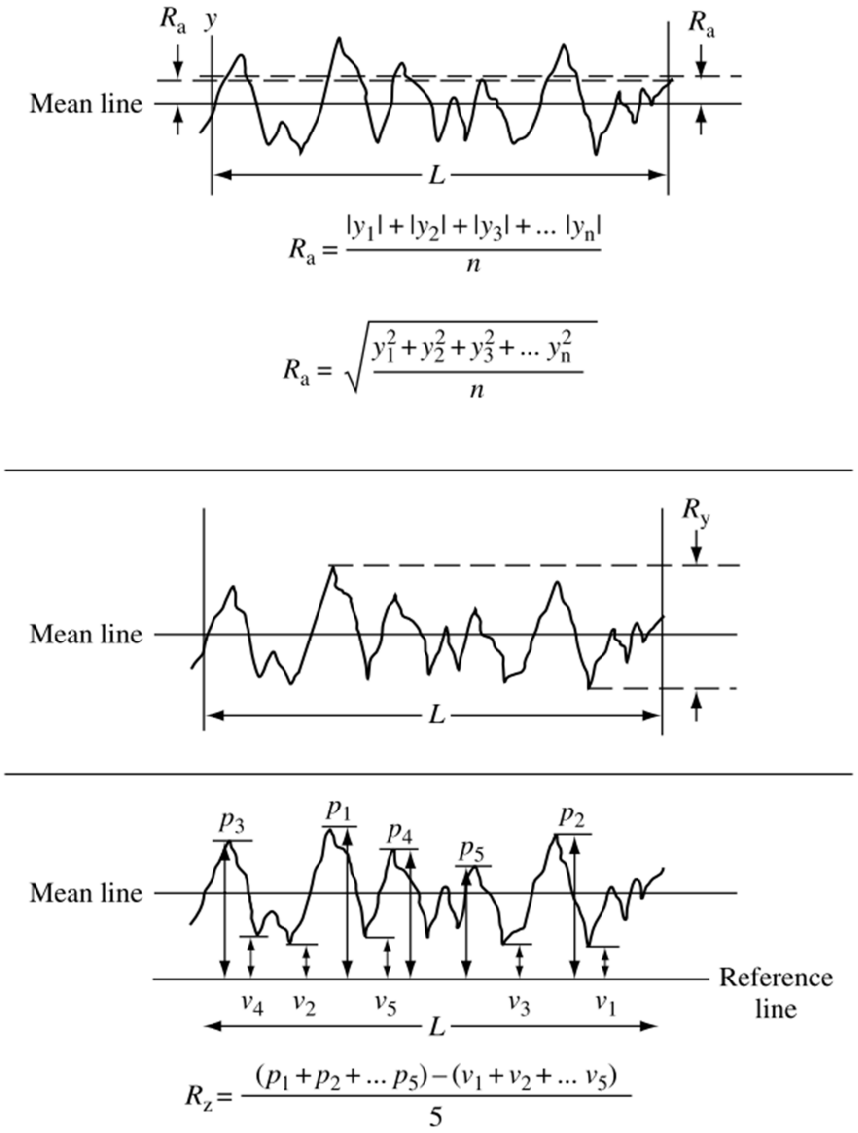

Figure 6.1. commonly used calculation for surface roughness mean value[27] (tabenkin, 1984)

Appendix D

***Table* 6-3** Bearing coefficient of friction

Bearing type	Coefficient of friction, μ
Deep-groove ball bearings	0.0015[a]
Self-aligning ball bearings	0.0010[a]
Angular-contact ball bearings	
Single row	0.0020
Double row	0.0024[a]
Four-point contact ball bearings	0.0024
Cylindrical roller bearings	
With cage	0.0011[b]
Full complement	0.0020[a,b]
Needle roller bearings	0.0025[a]
Spherical roller bearings	0.0018
Taper roller bearings	0.0018
Thrust ball bearings	0.0013
Cylindrical roller thrust bearings	0.0050
Needle roller thrust bearings	0.0050
Spherical roller thrust bearings	0.0018

[a] Applies to unsealed bearings.
[b] No appreciable axial load ($F_a \approx 0$).
Source: SKF (1999).

Appendix E

***Table* 6-4** Lubrication friction factor f_L for Equations

Bearing type	Grease lubrication	Oil spot lubrication	Oil bath lubrication	Oil bath with vertical shaft, oil jet
Deep-groove ball bearing	0.75–2	1	2	4
Self-aligning ball bearing	1.5–2	0.7–1	1.5–2	3–4
Angular-contact ball bearing				
Single row	2	1.7	3.3	6.6
Double row, bearing pair	4	3.4	6.5	13
Cylindrical roller bearing	0.6–1	1.5–2.8	2.2–4	2.2–4[a]
Needle roller bearings	12	6	12	24
Spherical roller bearings	3.5–7	1.75–3.5	3.5–7	7–14
Taper roller bearings				
Single row	6–3	6	8	8–10[a]
Paired single row	12	6	12	16–20[a]
Thrust ball bearings	5.5	0.8	1.5	3
Cylindrical roller thrust bearings	9		3.5	7
Needle roller thrust bearings	14		5	11
Spherical roller thrust bearings			2.4–5	5–10

Note: When a range of values is indicated, small values apply to light series bearings and large values to heavy series bearings.

[a] Value given for oil jet lubrication. Double for oil bath lubrication with a vertical shaft.

Source: Abstracted from SKF (1999).

Appendix F

***Table* 6-5** Representative values of viscosity–pressure index Z

Material	*Z*
Mineral oil, typical value	0.60
Synthetic oils	
PAO synthetic hydrocarbon	0.45
Polyglycol	0.37–0.40
Diester	0.47
Polyol ester	0.48
Polybutenes	0.91
Polymethylsiloxane	0.49
Castor oil	0.43
Rapeseed oil	0.42
Glycerol	0.18
Water	0.10
Water-glycol fluid	0.14

Source: Fein (1997).

Appendix G

We consider an incompressible , isothermal Newtonian flow (density ρ=const, viscosity μ=const), with a velocity field $\vec{V} = (u(x,y,z),\ v(x,y,z),\ w(x,y,z))$

Incompressible continuity equation:

$$\frac{\partial u}{\partial x} + \frac{\partial v}{\partial y} + \frac{\partial w}{\partial z} = 0 \qquad \textbf{eq1.}$$

Navier - Stokes equation:

vector form: $\rho \frac{D\vec{V}}{Dt} = -\nabla P + \rho \vec{g} + \mu \nabla^2 \vec{V}$

x component:

$$\rho\left(\frac{\partial u}{\partial t} + u\frac{\partial u}{\partial x} + v\frac{\partial u}{\partial y} + w\frac{\partial u}{\partial z}\right) = -\frac{\partial P}{\partial x} + \rho g_x + \mu\left(\frac{\partial^2 u}{\partial x^2} + \frac{\partial^2 u}{\partial y^2} + \frac{\partial^2 u}{\partial z^2}\right) \qquad \textbf{eq2.}$$

y component:

$$\rho\left(\frac{\partial v}{\partial t} + u\frac{\partial v}{\partial x} + v\frac{\partial v}{\partial y} + w\frac{\partial v}{\partial z}\right) = -\frac{\partial P}{\partial y} + \rho g_y + \mu\left(\frac{\partial^2 v}{\partial x^2} + \frac{\partial^2 v}{\partial y^2} + \frac{\partial^2 v}{\partial z^2}\right) \qquad \textbf{eq3.}$$

z component:

$$\rho\left(\frac{\partial w}{\partial t} + u\frac{\partial w}{\partial x} + v\frac{\partial w}{\partial y} + w\frac{\partial w}{\partial z}\right) = -\frac{\partial P}{\partial z} + \rho g_z + \mu\left(\frac{\partial^2 w}{\partial x^2} + \frac{\partial^2 w}{\partial y^2} + \frac{\partial^2 w}{\partial z^2}\right) \qquad \textbf{eq4.}$$

Cylindrical coordinates (r,θ,z)**:**

We consider an incompressible , isothermal Newtonian flow (density ρ=const, viscosity μ=const), with a velocity field $\vec{V} = (u_r, u_\theta, u_z)$.

Incompressible continuity equation:

$$\frac{1}{r}\frac{\partial (r u_r)}{\partial r} + \frac{1}{r}\frac{\partial (u_\theta)}{\partial \theta} + \frac{\partial u_z}{\partial z} = 0 \qquad \textbf{eq a)}$$

r-component:

$$\rho\left(\frac{\partial u_r}{\partial t} + u_r\frac{\partial u_r}{\partial r} + \frac{u_\theta}{r}\frac{\partial u_r}{\partial \theta} - \frac{u_\theta^2}{r} + u_z\frac{\partial u_r}{\partial z}\right)$$

$$= -\frac{\partial P}{\partial r} + \rho g_r + \mu\left[\frac{1}{r}\frac{\partial}{\partial r}\left(r\frac{\partial u_r}{\partial r}\right) - \frac{u_r}{r^2} + \frac{1}{r^2}\frac{\partial^2 u_r}{\partial \theta^2} - \frac{2}{r^2}\frac{\partial u_\theta}{\partial \theta} + \frac{\partial^2 u_r}{\partial z^2}\right] \qquad \textbf{eq b)}$$

θ-component:

$$\rho\left(\frac{\partial u_\theta}{\partial t} + u_r\frac{\partial u_\theta}{\partial r} + \frac{u_\theta}{r}\frac{\partial u_\theta}{\partial \theta} + \frac{u_r u_\theta}{r} + u_z\frac{\partial u_\theta}{\partial z}\right)$$

$$= -\frac{1}{r}\frac{\partial P}{\partial \theta} + \rho g_\theta + \mu\left[\frac{1}{r}\frac{\partial}{\partial r}\left(r\frac{\partial u_\theta}{\partial r}\right) - \frac{u_\theta}{r^2} + \frac{1}{r^2}\frac{\partial^2 u_\theta}{\partial \theta^2} + \frac{2}{r^2}\frac{\partial u_r}{\partial \theta} + \frac{\partial^2 u_\theta}{\partial z^2}\right] \qquad \textbf{eq c)}$$

z-component:

$$\rho\left(\frac{\partial u_z}{\partial t} + u_r\frac{\partial u_z}{\partial r} + \frac{u_\theta}{r}\frac{\partial u_z}{\partial \theta} + u_z\frac{\partial u_z}{\partial z}\right)$$

$$= -\frac{\partial P}{\partial z} + \rho g_z + \mu\left[\frac{1}{r}\frac{\partial}{\partial r}\left(r\frac{\partial u_z}{\partial r}\right) + \frac{1}{r^2}\frac{\partial^2 u_z}{\partial \theta^2} + \frac{\partial^2 u_z}{\partial z^2}\right] \qquad \textbf{eq d)}$$

Figure 6.2. Navier-Stokes equations